Report Title: Optimization of the Cathode Long-Term Stability in Molten Carbonate Fuel Cells: Experimental Study and Mathematical Modeling

Type of Report: Semiannual Progress Report

Reporting Period Start Date: October 1, 2001

Reporting Period End Date: March 31, 2002

Principal Author(s): Dr. Ralph E. White and Dr. Branko N. Popov

Date Report was Issued: April, 2002

DOE Award Number: DE-AC26-99FT40714 Modification A002

Name and Address of Submitting Organization:

Dr. Ralph E. White, Project Manager
Department of Chemical Engineering
University of South Carolina
Columbia, South Carolina 29208

DISCLAIMER

ABSTRACT

The dissolution of NiO cathodes during cell operation is a limiting factor to the successful commercialization of molten carbonate fuel cells (MCFCs). Lithium cobalt oxide coating onto the porous nickel electrode has been adopted to modify the conventional MCFC cathode which is believed to increase the stability of the cathodes in the carbonate melt. The material used for surface modification should possess thermodynamic stability in the molten carbonate and also should be electro catalytically active for MCFC reactions. Two approaches have been adopted to get a stable cathode material. First approach is the use of $LiNi_{0.8}Co_{0.2}O_2$, a commercially available lithium battery cathode material and the second is the use of tape cast electrodes prepared from cobalt coated nickel powders. The morphology and the structure of $LiNi_{0.8}Co_{0.2}O_2$ and tape cast Co coated nickel powder electrodes were studied using scanning electron microscopy and X-Ray diffraction studies respectively. The electrochemical performance of the two materials was investigated by electrochemical impedance spectroscopy and polarization studies.

A three phase homogeneous model was developed to simulate the performance of the molten carbonate fuel cell cathode. The homogeneous model is based on volume averaging of different variables in the three phases over a small volume element. The model gives a good fit to the experimental data. The model has been used to analyze MCFC cathode performance under a wide range of operating conditions.

TABLE OF CONTENTS

LIST OF GRAPHICAL MATERIALS

LIST OF TABLES

INTRODUCTION

Fuel cells may be expected, in the long term, to replace a major part of combustion system in all end use sectors, where they are, intrinsically clean [1]. One of the most promising electric power generation systems currently being sponsored by the US Department of Energy's National Energy Technology Laboratory is the molten carbonate fuel cell (MCFC). [2]. After having been under study and development for more than 40 years, MCFC are approaching the early stages of commercialization [3-5]. In fact, the start-up, testing and operation have been carried out in several pilot plants [6-9]. Nickel oxide is commonly used as the cathode material for molten carbonate fuel cells because of its activity and conductivity in the operation conditions. However, one of the major limits to the lifetime is the dissolution of the nickel oxide in the electrolyte resulting in a degradation of the cathode performance [10]. There is also a risk that dissolved nickel precipitates in the matrix on the anode side and causes a short-circuit of the cell. Attempts were made to solve this problem by looking for other materials. Previous work on $LiFeO_2$, Li_2MnO_3 and $LiCoO_2$ cathodes showed that electrodes made with these materials were chemically stable in the cathode environment because of the low dissolution rate [11-15]. However, the electronic conductivity was lower than that of NiO [16, 17]. Recently, new candidate materials such as LiCoO2 coated NiO [18] and pre-oxidized nickel-niobium surface alloy [19] have been proposed.

Based on previous investigations [20, 21] cobalt has been chosen to modify the surface of the NiO cathode and reduce its dissolution. Fukui *et al* [20] and Zhang *et al* [21] studied the effect of cobalt coating on nickel oxide particles used as cathodes in MCFCs. Ni particles were covered with CoO particles mechanically. Composites made of the Ni-CoO particles showed better corrosion resistance as compared to that of conventional NiO in Li-K carbonate melt. However, polarization characteristics of the Ni-CoO composite were not shown. Recently, Kuk *et al* [22] prepared $LiCoO_2$ coated NiO electrodes using cobalt electroplating followed by oxidation in molten Li and K carbonate electrolyte. Materials chosen for modifying the NiO surface should not affect the performance of the MCFC cathode. $LiCoO_2$ layers were formed on the internal surface of porous NiO electrodes by a solution impregnation technique using lithium hydroxide and cobalt hydroxide dissolved in acetic acid [23]. Nam *et al* also report a sol-gel coating of $LiCoO_2$ on NiO using acrylic acid as a chelating agent [23]. Zhang *et al* adopted a

solution dipping method for the formation of Ni/Co compound to increase the stability of MCFC cathodes [24]. In another approach Fukui *et al* coated cobalt oxide on to the Ni surface using a mechanofusion system to improve the cathode stability in molten alkali carbonate melt [20]. Earlier, micro-encapsulation of Co onto the porous nickel electrodes was carried out in our lab and it was evident from the results that this could be an alternate approach to fabricate a MCFC cathode material with enhanced stability in molten carbonate cathode working environment.

The MCFC cathode was stabilized by the electrodeposition of niobium onto nickel electrode followed by oxidation. It was found that under a cathode atm. of p(CO2)/p(O2) = 0.67 atm/0.33 atm, the equilibrium. solubility of nickel ions in (Li0.62, K0.38)2CO3 melt at 650^{o} C is about 17 ppm for the nickel oxide electrode and 8 ppm for the preoxidized nickel-niobium alloy electrode. The improvement in the stability of material in the melt may be attributed to the formation of a more dense nodular structure for the nickel-niobium alloy electrode when compared with a Ni electrode during pre-oxidation. As far as the thermal stability and the polarization performance are concerned, the pre-oxidized nickel-niobium alloy can be considered as a candidate for the cathode material of MCFCs [25, 26]. The *in-situ* oxidation of Ni-5 at. % Al and Ni-15 at. %Al alloys in molten Li and K carbonate melt were investigated by Mohamedi *et al* [27]. The period of the oxidation process depends on the aluminum content in the alloy. Ni-5 at. % Al electrode exhibited excellent stability during one-week immersion in the carbonate melts. Extension of cathode lifetime in molten carbonate fuel cells (MCFC) appears possible if the Ni cathode is modified by the addition of small concentration of aluminum. Thin films of $LiCoO_2$ or $LiMg_{0.05}Co_{0.95}O_2$ were prepared on a cathode body by a Complex Sol-Gel Process in order to protect them against dissolution [28]. A 350 hundred hours test in molten carbonates proved that the cathode bodies covered with $LiCoO_2$ are completely prevented from dissolution of Ni in a molten K/Li electrolyte. Dissolution of $LiCoO_2$ coating was not observed as well.

Hence the objective of this study is to prepare and characterize $LiNi_xCo_{1-x}O_2$ powders as a cathode material in molten carbonate fuel cells. Also, micro encapsulation of cobalt will be done on nickel powders, which will be used for the cathode preparation by aqueous tape casting process. For this, two different tape casting formulations will be prepared and cast as a green tape using doctor's blade. For the preparation of $LiNi_{0.8}Co_{0.2}O_2$ electrodes non-aqueous tape casting process employing xylene as solvent will be followed since the residual carbonate

precursors of lithium, nickel and cobalt caused agglomeration of the casting slurry when water is used as solvent for the slurry preparation. For the preparation of green electrodes from Co microencapsulated powders, aqueous tape casting will be employed. The prepared electrodes will be tested for its stability in molten alkali carbonate melt in cathode atmosphere. Also, the half-cell performance will be evaluated.

First principles based theoretical models for MCFC cathode can be divided into the thin film model [29] and the agglomerate model [30]. The principal deficiency of the agglomerate model, apart from the simplified pore structure assumed, is the lack of measured values for film thickness and agglomerate radius. Both these parameters cannot be estimated appropriately.

The problems associated with the agglomerate model can be avoided if we take the alternate approach, namely the volume averaging technique used for porous media as done by Prins-Jansen *et al* [31] and De vidts and White [32]. As compared to the agglomerate model where macropores and micropores remain as separate entities, in this approach the pores in the electrode exist in a single continuum. Further, all three phases co-exist within the porous electrode and reaction proceeds everywhere at the solid/melt interface. Using the volume averaging technique, Prins-Jansen *et al.* [31] developed an impedance model for extracting the reaction and transport parameters from experimental data. The model developed by Prins-Jansen *et al.* [31] combines both the electrolyte and gas phases into a single entity during volume averaging. The gas and liquid phase mass transport were not considered separately. In this report, we adopt the volume averaging technique as outlined by De vidts and White [32] for three phase reactions in porous electrodes. Using this approach, volume averaged concentrations of both gaseous and liquid phase reactants are obtained separately.

In the previous report the development of three-phase homogeneous model of the molten carbonate fuel cell cathode was presented. The concepts of volume averaging and derivation of model equations using volume averaging were presented in detail along with brief discussion on the effect of parameters. In this report we look at the results of the model and the fitting to experimental data.

EXECUTIVE SUMMARY

- Two approaches have been adopted to get a stable cathode material. First approach is the use of $LiNi_{0.8}Co_{0.2}O_2$, a commercially available lithium battery cathode material and the second is the use of tape cast electrodes prepared from cobalt coated nickel powders.
- SEM analysis on $LiNi_{0.8}Co_{0.2}O_2$ electrodes sintered at 800°C show good pore structure. Pore volume distribution studies done using mercury porosimetry showed lower porosity when compared to that of state-of-the-art cathode.
- The i-V characteristics of $LiNi_{0.8}Co_{0.2}O_2$ are good offering a current drain of 160 mA/cm^2 for a voltage polarization (IR free) of 140 mV
- Long-term stability tests revealed that Cobalt coated Nickel electrode has a lower solubility in molten alkali carbonate melts when compared to the state-of-the-art nickel oxide cathodes.
- A three phase homogeneous model based on the concept of volume averaging has been developed for the MCFC cathode.
- The cathode performance is studied for different conditions using model simulations.
- The diffusion coefficients, electrolyte conductivity and the exchange current density have an Arrhenius form of dependency on temperature. This relationship is obtained by fitting the experimental data of $LiNiCoO_2$ to the model at different temperatures.

EXPERIMENTAL

(a) $LiNi_{0.8}Co_{0.2}O_2$

Preparation of Electrodes: Cobalt doped lithium nickel oxides were prepared using solid-state synthesis procedure. Stochiometric amounts of lithium nitrate ($LiNO_3$), nickel hydroxide ($Ni(OH)_2$) and cobalt oxalate ($CoC_2O_4.2H_2O$) obtained from Aldrich chemical company were used as the starting precursors for the solid-state synthesis. The compounds were mixed thoroughly and were heated in the presence of helium (regular grade, National Welders) at 250°C first for about 5 hours followed by heating at 630°C for 2 days. All the temperature ramps were maintained at 1°C/min. After the helium treatment, the samples were heated in oxygen atmosphere at 800°C for 20 hours. Following this, the samples were finally heated in an autoclave at 500 psi O_2 pressure at 700°C for 20 hours. Figure 1 shows the scanning electron micrographs of synthesized $LiNi_xCo_{1-x}O_2$. As the cobalt doping is increased from 0.1 to 0.2, a significant increase of $LiNi_xCo_{1-x}O_2$ particle size is observed. However the particle size did not change significantly between cobalt doping of 0.2 to 0.3.

Tape casting: - Porous $LiNi_{0.8}Co_{0.2}O_2$ cathodes were made by a tape casting and sintering process. $LiNi_xCo_{1-x}O_2$ particles (synthesized by solid-state reaction) were ground and sieved to obtain uniform particles of size 3-5 μm. The tape casting slurry was prepared by ball milling $LiNi_xCo_{1-x}O_2$ powder in xylene with suitable binder (poly vinyl butyral - PVB) and plasticizer (benzyl butyl phthalate and poly ethylene glycol 50-50 vol.% mixture). The ball milling was done in two steps. At the first step, 50 g of $LiNi_xCo_{1-x}O_2$ were added to 0.5 g of dispersant (GTO). The ingredients were mixed thoroughly with 32 ml of Xylene and the slurry was ball milled for 6 hr in order to break the weak agglomerates. Xylene was selected as a solvent because mixed solvent system like methyl ethyl ketone (MEK), ethanol caused skinning of the cast surface due to quick evaporation of ethanol. Next, 6 g of PVB and 4 ml of plasticizer mixture was added to the above suspension and the resulting slurry was ball milled for an additional 6 hr. The slurry was then cast using a doctor blade assembly over a glass plate. The drying was performed slowly at room temperature for about 48 hours. The cast plate $LiNi_{0.8}Co_{0.2}O_2$ tape is then stripped off gently from the glass plate and stored.

Sintering: Sintering of the tape cast electrodes influences the cathode pore structure and thereby affects its electrochemical performance. TGA was done to determine the optimum heat treatment

schedule for sintering. A typical TGA curve for green $LiNi_{0.8}Co_{0.2}O_2$ tape is shown in Figure 2. The as cast $LiNi_{0.8}Co_{0.2}O_2$ tape was pre-heated at 150°C for 12 hours in order to remove all the solvent in the tape. TGA analysis was done by heating the sample from 100°C to 650°C at a rate of 10°C/min. A steep reduction in weight (12 wt%) is seen on heating the sample between 200 and 400°C due to the removal of the binder and plasticizer. The removal of all volatile and decomposable organic matter is completed below 400°C. The total weight loss varies between 13 to 15wt.% depending upon the binder and plasticizer contents in the green tapes. Figure 3 shows the scanning electron micrographs of $LiNi_{0.8}Co_{0.2}O_2$ tapes sintered at 750°C, 800°C, 850°C and 900°C. Tapes sintered at 800°C showed better pore structure. Based on the above TGA and SEM analysis, the following heating pattern was used - for sintering the electrodes: (i) green tapes which were cut out to specific area (10 cm x 10 cm) were initially heated from room temperature - to 150°C at a rate of 1°C/min in air, (ii) in the second step the temperature was held at 150°C for 10 hours, (iii) next, the temperature was raised to 400°C at a rate of 1°C/min in air, (iv) the temperature was held at 400°C for 3 hours, (v) the temperature was raised to 800°C at 1°C/min in air, (vi) the temperature was held at 800°C for 1 hour and (vii) in the last step the sample was cooled to room temperature using a cooling rate of 1°C/min.

Pot cell studies: - In order to determine the solubility of $LiNi_{0.8}Co_{0.2}O_2$, pot tests were carried out under cathode gas conditions. Pellet electrodes of 1 cm diameter were made by pressing the $LiNi_{0.8}Co_{0.2}O_2$ powders obtained using solid-state reaction. They were weighed and carefully dropped inside an alumina crucible containing 100 g of molten carbonate (Li_2CO_3/K_2CO_3=62/38) at 650°C. Cathode gas (30% CO_2/70% air) was bubbled through the carbonate melt using alumina tubes. About 0.5 g of molten carbonate was taken from the melt approximately every 6 hours up to 200 hours using an alumina rod. The molten carbonate sample was dissolved in 10% dilute acetic acid. Atomic absorption spectroscopy was used to analyze the concentration of dissolved nickel.

Electrochemical and Material Characterization: - Half-cell performance studies were done in a 3-cm^2-lab cell shown in Ref. [28]. $LiNi_{0.8}Co_{0.2}O_2$ was used as the working and counter electrodes. $(Li_{0.62}K_{0.38})_2CO_3$ eutectic embedded in a $LiAlO_2$ matrix was used as the electrolyte. Polarization studies were done using an oxidant gas composition of 70% air and 30% CO_2. Two oxygen reference electrodes ($Au/CO_2/O_2$) connected to the electrolyte tile with a salt bridge

($50\%(Li_{0.62}K_{0.38})_2CO_3$ + $50\%LiAlO_2$) were used to monitor the polarization of cathode. Electrochemical impedance spectroscopic studies were performed using a Model 1255 Schlumberger Frequency Analyzer. The electrode was stable during the experiments and its open circuit potential changed less than 1 mV. The impedance data generally covered a frequency range of 1 mHz to 100kHz. A sinusoidal ac voltage signal varying by ± 5 mV was applied in all cases. X-ray diffraction (XRD) was used to study the crystal structure of the samples. Mercury porosimeter was used to characterize the pore-volume distribution of the sintered cathodes.

RESULTS AND DISCUSSION

X-ray diffraction studies: - Figure 4 shows the typical powder X-ray diffraction patterns of pristine $LiCoO_2$ and $LiNi_xCo_{1-x}O_2$ solid solutions. These patterns reveal that all these materials are single phase with the α-$NaFeO_2$ structure, space group R3*m*. The transition metal ions are in turn surrounded by six oxygen atoms. Infinite layers of $Ni_xCo_{1-x}O_2$ were formed through edge sharing of the ($Ni_xCo_{1-x}O_6$) octahedras, with the intercalating lithium ions located between the layers. All of the diffraction lines of $LiNi_xCo_{1-x}O_2$ can be indexed with a hexagonal lattice. Analytical results were obtained from the XRD data using the lines (0, 0, 3) and (1, 0, 4). As the Ni^{3+} ions at the 3(a) sites of the $LiNiO_2$ lattice are partially replaced by Co^{3+} ions, the unit cell dimensions, a and c, in a hexagonal setting become smaller. The lattice constants were a = 2.876 Å and c = 14.183 Å for $LiNi_{0.9}Co_{0.1}O_2$; a = 2.871 Å and c = 14.176 Å for $LiNi_{0.8}Co_{0.2}O_2$; a = 2.865 Å and c = 14.170 Å for $LiNi_{0.7}Co_{0.3}O_2$ and a = 2.816 Å and c = 14.046 Å for $LiCoO_2$. This decrease in lattice constants is due to the difference in size between trivalent cobalt and trivalent nickel ions ($r_{Ni}^{3+} = 0.56$ Å, $r_{Co}^{3+} = 0.53$ Å) [33]. These results strongly suggest that $LiNi_xCo_{1-x}O_2$ is in a homogenous phase, i.e. Ni^{3+} and Co^{3+} are homogenously located at the octahedral 3(*a*) sites in a cubic phased oxygen array.

Figure 5 compares the XRD patterns of $LiNi_xCo_{1-x}O_2$ sintered at 800°C for a period of 24 h in the presence of air. The XRD patterns indicate that the (0, 0, 3) line characteristic of the lithium content decrease for the case of $LiNi_{0.9}Co_{0.1}O_2$. As the cobalt content increases in the

$LiNi_xCo_{1-x}O_2$ (x = 0.2, 0.3, 1), the lithium evaporation on heating also decreases. Perez et al [34] carried out a similar experiment wherein they treated different Li(NiCo) mixed oxides in molten carbonate at 650°C under air and observed a decrease in lithium content in the oxides. Figure 6 compares the XRD patterns of $LiNi_{0.8}Co_{0.2}O_2$ heat treated at different temperatures for a period of 24 h. It is seen that the $LiNi_{0.8}Co_{0.2}O_2$ is quite stable upto sintering temperatures of 800°C in terms of lithium content. Heating $LiNi_{0.8}Co_{0.2}O_2$ to 1100°C leads to a lot of lithium loss, which is seen, from the different XRD pattern obtained. Also, XRD pattern obtained from $LiNi_{0.8}Co_{0.2}O_2$ samples heat treated in molten carbonate for 500 hours under air at 650°C shows no significant structural change when compared to pristine oxide. This results show that $LiNi_xCo_{1-x}O_2$ (x = 0.2, 0.3) may exhibit the structural integrity needed of a MCFC cathode to sustain long-term operation.

Scanning Electron Microscopy: SEM of $LiNi_{0.8}Co_{0.2}O_2$ electrodes sintered at different temperatures is shown in Fig. 3. It is evident that the electrodes sintered at 800^o C showed good pore structure when compared to the other electrodes sintered at 850^o, 900^o and 1000^o C respectively. At temperatures higher than 800^o C, the electrode seems to be more sintered and melting of the electrode started at around 1000^o C. Therefore, the sintering temperature was optimized at 800^o C.

Stability tests: - The short-term stability of $LiNi_xCo_{1-x}O_2$ (x = 0.1, 0.2, 0.3) in molten carbonate eutectic was determined using pot tests. Atomic absorption (AA) was used to analyze the dissolved nickel in the melt. Figure 7 shows the results of AA analysis on the amount of dissolved nickel in the carbonate melt as a function of time. The results indicate that cobalt doping increases the resistivity of the oxide to the molten carbonate environment. The amount of nickel and cobalt cation in the carbonate melt increases with time and saturates after about 100 hours. This dissolution rate obtained for $LiNi_xCo_{1-x}O_2$ is about one half of the dissolution of state-of-the-art nickel oxide reported in literature [22-26]. Based on these results and the XRD data, it was decided to carry out further studies on $LiNi_{0.8}Co_{0.2}O_2$. These compounds exhibit enough stability at operating temperatures and also the rate of dissolution of nickel is lower when compared to state-of-the-art cathodes.

Pore volume distribution: - The electrode structure is one of the principal factors determining cell performance in MCFCs. The electrode reaction takes place mainly near the meniscus (three phase boundary), where mass transport resistance is least for gas diffusing through the liquid to

the reaction surface. Alternatively an electrolyte film may cover the pore wall through which the gas diffuses to the electrode. Flooding of the electrode is usually deleterious to the performance of cathodes. Cathode porosity is adjusted in order to ensure proper electrolyte distribution. Small pores retain electrolyte by capillary pressure, while large pores are gas-filled, even though their walls may be fully or partly wetted by thin liquid films. Figure 8 shows the pore volume distribution of sintered $LiNi_{0.8}Co_{0.2}O_2$ cathodes. The pore size distribution shows three kinds of pores ranging from micro pores of less than 1 μm size to macro pores of size greater than 10 μm. Majority of the pores lay in the intermediate class of particle size around 2~3 μm. The porosity of the sintered $LiNi_{0.8}Co_{0.2}O_2$ cathode was 38.5311%. This value is lower when compared to the porosity of *in-situ* sintered state-of-the-art NiO cathode (porosity~50-55%) [34, 35]. This low porosity in case of $LiNi_{0.8}Co_{0.2}O_2$ cathode can cause higher polarization during testing of these electrodes. However, porosity can be enhanced by the addition of pore formers during tape casting and by careful optimization of sintering conditions.

Polarization studies: -Polarization studies were carried out in a three electrode 3 cm^2 lab scale cell containing $LiNi_{0.8}Co_{0.2}O_2$ electrodes both as the working and counter electrodes Gold (oxygen reduction) served as a reference electrode. The electrodes were separated by a $LiAlO_2$ ceramic tile containing Li/K carbonate melt (62-38mol%). The cell is connected to a gold/oxygen reference electrode through a salt bridge. The polarization characteristics $LiNi_{0.8}Co_{0.2}O_2$ cathodes were obtained by varying the current load. Figure 9 compares the cathode polarization during the galvanodynamic scan for the LiNi0.8Co0.2O2 electrode at different operating temperatures. The current was scanned at 1 mA/sec and the curves have been corrected for IR loss based on R_Ω calculated from impedance measurements (not shown).

The i-η characteristics of $LiNi_{0.8}Co_{0.2}O_2$ cathodes obtained at different temperatures are similar to each other indicating two regions; charge transfer at lower overpotentials and a complex mass transfer and charge transfer limited process at higher overpotentials. Increasing the temperature has a significant influence on the polarization in case of $LiNi_{0.8}Co_{0.2}O_2$. The observed overpotentials η decrease with increasing the temperature indicating a decrease of both the polarization and diffusion overpotentials with an increase of temperature. The voltage polarization decreased from 140 mV at 160 mA/cm^2 in case of 650°C to 65 mV/cm^2 at 750°C as shown in Fig 9. Similar results were observed in literature in case of NiO electrodes [34,36,37]. Our earlier study showed a voltage polarization of 55 mV for NiO and 95 mV for Co

encapsulated nickel electrodes for an applied current of 160 mA/cm^2. Fig. 10 shows the effect of temperature on cathode polarization of NiO and Co encapsulated NiO. This difference in the performance of $LiNi_{0.8}Co_{0.2}O_2$ and NiO cathodes can be attributed to the poor porosity (~45%) of the $LiNi_{0.8}Co_{0.2}O_2$ cathodes.

The performance of the $LiNi_{0.8}Co_{0.2}O_2$ electrodes was evaluated from the exchange current density data obtained from i-V plots under low current load ($i \leq 10$ mA/cm^2). The slope of the linear part of i-V curve was used to calculate the apparent exchange density based on the expression $i_o = \frac{RT}{nFR_{ct}}$ where, R is the universal gas constant, T is the cell temperature, F is the Faraday's constant and R_{ct} is the slope of the i-V response. The range of values of exchange current density calculated for $LiNi_{0.8}Co_{0.2}O_2$ cathodes varied from 25.1 to 26.1 mA/cm^2 during various stages of operation. The apparent exchange current density calculated using the same method for the case of NiO in one of our earlier studies varied between 29–31 mA/cm^2 [38]. The low exchange current density observed could again be due to the lower porosity in case of $LiNi_{0.8}Co_{0.2}O_2$ cathodes.

Electrochemical Impedance Spectroscopy (EIS) studies: - In order to understand the kinetics of oxygen reduction on $LiNi_{0.8}Co_{0.2}O_2$, impedance measurements were carried out at different gas compositions. EIS analysis was carried out at open circuit on the $LiNi_{0.8}Co_{0.2}O_2$ electrodes. Figure 10 shows the impedance analysis of NiO and $LiCoO_2$ electrodes at different temperatures at a particular gas composition. The impedance response at any given temperature is characterized by the presence of high frequency loop and an extension at low frequencies. The high frequency plot has been associated with the charge transfer processes while the low frequency loop to a slow process (mass transfer or slow homogeneous reactions). The impedance response shown in Fig. 11 (a, b, c, d, e and f) is similar in appearance to the ones obtained by Yuh *et al*. [36,37] under similar conditions for NiO cathodes. As shown in Figure 11, the cell temperature has a marked effect on the ac impedance. Increasing the temperature, a drastic decrease of charge transfer resistance is seen, which in agreement with the results obtained from polarization studies.

From Figures 12 (a, b, c, and d), it can also be seen that the effect of partial pressure of O_2 and CO_2 are antagonistic to each other. The magnitude of the impedance loop decreased on increasing the O_2 partial pressure. This clearly indicates a positive reaction order for oxygen and

is similar to the response seen for NiO [20]. In case of CO_2, the impedance value increased with an increase in CO_2 partial pressures implying that the reaction order of CO_2 must be negative. Yuh *et al.* [37] obtained similar results for NiO in terms of O_2 and CO_2 dependence on impedance responses. This shows that oxygen reduction kinetics in $LiNi_{0.8}Co_{0.2}O_2$ follows a similar mechanism as in that of NiO. Hence $LiNi_{0.8}Co_{0.2}O_2$ can be used as a cathode material for MCFC applications.

(b) Preparation of cobalt coated nickel electrodes

Porous cobalt coated nickel cathode was made by a tape casting and sintering process. Cobalt micro-encapsulation on nickel particles was done by a method developed in our laboratory. The tape casting slurry was prepared by ball milling cobalt coated nickel powder (3-5 μm) in water with suitable binder (PVA) and plasticizer (glycerol). The ball milling was done in two steps. At the first step, 50 g of nickel powder were added to 0.50g of dispersant (Disperbyk-112, BYK Chemie) and milled in de-ionized water for 24 h. After the first de-agglomeration step, 8-10 wt % PVA powder was added and milled for 12 h with a defoamer (Airdefoam™ 60, Air Products). After this step, glycerol was added and milled for another 12 h. The slurry was filtered and then cast using a doctor blade assembly over a glass plate coated with silicone oil. The drying was performed slowly at room temperature for about 48 hours. The cast cobalt coated nickel tape is then stripped off gently from the glass plate and stored. The green tapes were sintered in a programmed manner at 875^o C under reduced atmosphere.

Material and Electrochemical characterization: Scanning electron microscopy was used to see the surface morphology changes after sintering and after immersion in molten carbonate melt. X-Ray diffraction study was used to confirm the final compound formed after cell testing. The half-cell performance of the tape cast cobalt coated electrode was studied in a laboratory scale 3 cm^2 cell using the same as both working and counter electrodes. The working and counter electrodes were separated by $LiAlO_2$ matrix embedded with Li and K carbonate eutectic mixture (62:38 mol%). Gold wire inserted in an alumina tube was served as the reference electrode ($Au/CO_2:O_2$). The bottom portion of the alumina tube was filled with $LiAlO_2$ and $(Li_{0.38} + K_{0.62})$ CO_3 (50:50 wt%) paste prepared at 650^o C. This set-up facilitates good contact through a salt bridge. Electrochemical impedance spectroscopic studies were performed using a Model 1255 Schlumberger Frequency Alalyzer. The impedance data covered a frequency range of 1 mHz to 100 kHz. A sinusoidal voltage varying by ± 5 mV was applied in all studies.

Results and discussions:

(a) Scanning electron Microscopy: Fig. 13 shows the SEM images of green tape, sintered electrode and the electrode after immersion in molten carbonate melt for 24 h. Green tape sintered in H_2 atmosphere shows a good electrode network needed for an MCFC cathode. No much difference was noticed on the morphology and grain size of H_2 sintered electrode and the electrode immersed in molten carbonate melts.

(b) Electrochemical impedance spectroscopic (EIS) studies: The oxygen reduction kinetics was studied using impedance technique at three different operating temperatures under different gas compositions. EIS was carried out at equilibrium potential (open circuit) on tape cast Co coated nickel electrodes. Fig. 14 shows the impedance response of Co-Ni electrode at 650^o C under different gas compositions.

Effect of CO_2 partial pressure: Fig. 14 (a) shows the influence of CO_2 partial pressure on the impedance behavior of Co-Ni electrodes at 650^o C. It was clearly seen that the both the low and high frequency arcs increases as the CO_2 partial pressure increased. This indicates that the process of charge transfer is affected as the CO_2 partial pressure is increased. Moreover the total magnitude of the impedance is increased while increasing the CO_2 partial pressure. This suggests that the reaction order for CO_2 must be negative. As the temperature increases, the impedance magnitude decreased. This is due to the faster kinetics at higher temperatures and also due to the decreased solution resistance.

Effect of O_2 partial pressure: The dependence of O2 partial pressures on the impedance behavior is shown in Fig. 14(b). The low frequency arc of the impedance spectra is decreased while increasing the O2 partial pressure. This suggests that the oxygen reduction process is influenced by the O_2 partial pressures. Also, the arcs at high frequency region of the impedance spectra are not influenced by the O_2 partial pressures. Increase in O_2 partial pressure caused decrease in the total magnitude of impedance indicating a positive reaction order for O_2. The magnitude of the impedance curve decreased at temperatures above 650^o C, indicating faster reaction kinetics and lesser electrolyte resistance. The effect of temperature is shown in Fig. 14 (c, d, e & f).

Impedance behavior with time: The impedance behavior of cobalt coated tape cast nickel electrode with time is presented in Fig. 15. Initially the electrode showed a single impedance arc 10 hours after reaching the operating temperature of 650^o C. The second arc due to the mass

transfer reaction is observed nearly after 20 hours. This may be due to the fact that the cell might not have reached its equilibrium. Initially, steady increase of the lower frequency arc is observed. This may be due to the slower mass transfer reactions. This caused higher impedance value up to 60 hours and after that decrease in impedance magnitude was observed. This shows that the electrode needs some time to get oxidized completely. A steady increase in the impedance values was observed after 82 hours. This may be due to the loss in electrolyte in the cell. In all the cases two distinguish arcs are observed; the higher frequency arc is due to the charge transfer process and the low frequency is due to the mass transfer processes.

Cell assembly and testing: Laboratory scale 3cm^2 cells were assembled using Ni-10 wt. % Cr anode, developed cathode and $LiAlO_2$ matrix embedded with Lithium and potassium carbonate eutectic melt (62:38 mol%). The cell was held at 510^o C for 10 hours to enable all the components to be filled with the electrolyte. Full cell performance of the developed cathode material is under investigation.

Mathematical Modeling of the MCFC Cathode: Next, we develop a theoretical model to simulate the performance of the MCFC cathode. The model is used to extract kinetic and thermodynamic parameters associated with different cathode materials. The model equations have been solved simultaneously using Femlab 2.1 and also using Newman's Band(j). In studying the performance of the cathode, the main parameter of interest is the electrode polarization under different applied currents. The measured polarization is the difference in potential between the current collector $(\Phi_M)_o$ under load as compared to at open circuit $(\Phi_M)_{o,OCV}$. However, the model solves for the local overpotential ϕ, which is the difference between the solid phase and liquid phase potential. Lee *et al.* [39] present a relationship between this overpotential and the experimentally measured polarization loss (Φ_{Mo}-$\Phi_{Mo,OCV}$). The IR free polarization is given as,

$$\phi_{IR-free} = (\Phi)_0 + \frac{1}{1+\kappa_{app}/\sigma_{app}}\left[(\Phi)_L - (\Phi)_0\right] \qquad (1)$$

where κ_{app} and σ_{app} are the apparent conductivities modified by the porosity. Using the model we studied the effect of different parameters on the IR free polarization loss.

Effect of Conductivity and Exchange Current Density:

Model simulations show that increase in κ decreases the polarization loss electrode for different κ values. When the electrolytic and ohmic conductivities are equal to each other a symmetrical

reaction rate distribution curve is obtained. This is similar to the analysis given by Newman [40] for porous electrodes. Although a uniform reaction distribution is the desirable scenario practical considerations limit us from achieving this. In general solid phase conductivities are much larger than liquid phase conductivities. Hence, the actual electrode utilization is not 100% but much lower than that. Using this theoretical model it is possible to optimize the electrode thickness based on input electrode parameters.

In the previous report we showed that at high values of i_o the polarization loss increases linearly with increasing applied loads. However, at low values of i_o the polarization loss increases asymptotically and reaches a plateau with increase in current. Overpotential profiles for different exchange current densities showed that the overpotential increases sharply near the separator side of the electrode. It can also be seen that the large potential drop close to the electrolyte matrix increases with decrease in i_o. The variable di_2/dx is a measure of the reaction rate or the current transferred per unit volume ($a^{(sl)}j_k$). If the reaction rate (di_2/dx) in a region is about 5% or less than the maximum reaction rate then that part of the electrode material is considered inactive. The percent utilization of the active material is calculated for different i_o using this baseline (5% of the maximum reaction rate). Figure 16 shows the percent utilization of the electrode material as a function of the exchange current density. It can be clearly seen that as i_0 increases the utilization decreases indicating that only a small fraction of the active material takes part in the reaction. Most of the reaction takes place in a small part of the electrode near the separator. From Fig. 16 it can be seen that increase in i_o translates to poor utilization of active material. For small i_o values the reaction rate is slow and hence this allows sufficient time for dissolved O_2 and CO_2 to reach the active solid interface and react. The slow reaction rate also allows the reaction to take place much deeper within the electrode as compared to at high reaction rates. Both these factors contribute to the higher utilization observed for low i_o values.

Effect of diffusion coefficient:

It can be seen that change in liquid phase diffusion coefficient significantly alters the concentration across the electrode. At very low values (10^{-4} cm^2/s) of $D_{i,l}$ the O_2 and CO_2 concentration close to the matrix drops to zero (not shown in figure). However, the diffusion coefficient for both dissolved oxygen and carbondioxide in MCFC cathodes lies in the order of 10^{-3} – 10^{-2} cm^2/s [31]. From simulations it can be seen that at this value of the diffusion

coefficient no depletion of dissolved CO_2 occurs anywhere within the electrode. However, it can be seen clearly that a concentration gradient exists across the thickness of the electrode. Similar results are seen for oxygen also. The overpotential is almost uniform for large diffusion coefficients whereas for small diffusion coefficients the overpotential increases drastically very near the separator region. A similar effect is seen for both O_2 and CO_2. Also, simulation results show that changing the diffusion coefficient by one order of magnitude results in an increase in polarization of only 20 mV. This effect is smaller than that seen for electrolyte conductivity and exchange current density. These results indicate that mass transfer in the liquid phase is not rate limiting for MCFC cathodes.

Effect of thickness of the electrode:

The resistance to mass transfer increases as the electrode thickness increases. Hence the polarization increases with the thickness. Increasing the thickness has two conflicting effects, both the mass transfer resistance and the active surface area are being increased. Due to this competing effect, the polarization loss should go through an optimum as the electrode thickness is increased. However in our model simulations and in Prins-Jansen *et al.* [30] we observe a monotonic dependency where polarization loss always increases with increase in thickness. This can be attributed to the assumption involved in the model simulation i.e. the active surface area does not change with increase in thickness.

Fontes *et al.* [41] state that optimum electrode thickness is shifted towards thicker electrodes as the catalyst conductivity increases. Increase in the electrolyte conductivity increases the utilization of the active material. Hence the thickness of the electrode can be increased with increased electrolyte conductivity to obtain similar performance. Figure 17 plots the CO_2 gas phase concentration across the electrode thickness. It can be seen that even under high utilization (40% - 60%) all the gas in the electrode is not consumed. For an electrode thickness of 0.8 mm close to 40% of the inlet gas is still available at the outlet. In MCFC stacks, it has been estimated that the utilization of the oxidant gases is only around 40%. This indicates that the change in gas phase concentration does not have a significant effect on the electrode performance at high gas flow rates. However, decrease in both oxygen and carbondioxide flow rate will affect the performance of the cathode. The liquid phase reactant concentrations are directly dependent on the gas concentration in the macropore at that point. Low flow rates

contribute to high utilization thereby leading to a decrease in gas phase concentration. This will decrease the amount of reactant available for taking part in the reduction reaction at the solid/liquid interface and hence increase the polarization loss.

Comparison of model to experimental data

Figure 18 compares the model to our experimental data of $LiNiCoO_2$ at different temperatures. With increase in temperature the reaction rate as given by the exchange current density and the species transport rate as given by the diffusion coefficient increase. Further the electrolyte conductivity also increases. The gas phase diffusion coefficients at different temperatures can be calculated using the Chapman-Enskong equation [42]. The temperature dependency of the liquid phase diffusion coefficients, electrolyte conductivity and the exchange current density were determined by fitting the model to the experimental data. In all cases an Arrhenius relationship to the temperature was obtained. The fitting results along with the R^2 term are given in Table II. The dependence is given by

$$x = a \exp\left(-\frac{b}{T}\right)$$

The parameters obtained from fitting the model data were used in the subsequent simulations. Our next goal was to compare the polarization behavior of the cathode under different gas compositions.

Our model predicts monotonic dependence of the polarization loss on both CO_2 and O_2 partial pressure. The exchange current density is concentration dependent and has negative reaction order dependence for CO_2 and a positive order dependence for O_2. Increasing the concentration of CO_2 decreases the local current density and hence increases the polarization. The effect is the reverse for O_2. Similar results have been obtained by previous researchers also. This is shown in Fig. 19, which gives the fit of our model to experimental data of $LiCoO_2$ obtained by Lagergren and Simonsson [43] for different gas compositions. The model parameters remained the same as for $LiNiCoO_2$ (see Table II) except for the exchange current density, which was calculated as 5 mA/cm^2 at 650^oC.

Kunz and Murphy [44] have shown experimentally that when the amount of nitrogen inert in the cathode inlet gas increases the polarization drop increases. This is attributed to the increased gas-phase mass transfer resistance as nitrogen partial pressure increases. Model

simulations with different inlet N_2 concentrations are shown in Fig. 20. The polarization drop increases with decreased O_2 and CO_2 concentration for different current densities.

Figure 21 presents comparison of polarization profiles between three different cathode materials namely, NiO, $LiCoO_2$ and $LiNiCoO_2$. For all three cathode materials good agreement is seen between model simulations and experimental data. NiO is a p type semiconductor and has a lower conductivity than pure Ni. Li^+ ions coming from the electrolyte diffuse into the NiO and increase its electronic conductivity. However, NiO has much larger exchange current density for oxygen reduction as compared to alternate cathode materials such as $LiNiCoO_2$ and CoO_2**.** Model simulations indicate that an electrode made of a material, which has the conductivity of NiO, and exchange current density of $LiCoO_2$ would suffer around 100% more polarization than the conventional NiO cathode. The exchange current density and electrode conductivity of the three materials obtained using the homogeneous model are given in Table III. These results show that the model can be used to extract critical thermodynamic, kinetic and transport parameters from polarization data.

CONCLUSIONS

$LiNi_xCo_{1-x}O_2$ was synthesized by solid-state reaction from lithium nitrate, nickel hydroxide and cobalt oxalate precursors. Lithium loss occurred during sintering of these mixed oxides and this loss gradually decreased with the increase in cobalt content. $LiNi_xCo_{1-x}O_2$ show lower rate of dissolution in molten carbonate under cathode gas conditions when compared to that of NiO listed in literature. The rate of dissolution decreased with increase in cobalt content. However, considering the economy of cobalt doping, and stability at higher temperatures, $LiNi_{0.8}Co_{0.2}O_2$ was chosen for further characterization studies. $LiNi_{0.8}Co_{0.2}O_2$ cathodes for MCFC were made by a tape casting and sintering process. SEM analysis on $LiNi_{0.8}Co_{0.2}O_2$ electrodes sintered at 800°C show good pore structure. Pore volume distribution studies done using mercury porosimetry showed lower porosity when compared to that of state-of-the-art cathode. The i-V characteristics of $LiNi_{0.8}Co_{0.2}O_2$ are good offering a current drain of 160 mA/cm^2 for a voltage polarization (IR free) of 140 mV. Impedance spectroscopic studies done on $LiNi_{0.8}Co_{0.2}O_2$ under different gas conditions indicate that the oxygen reduction reaction mechanism follows a positive order for O_2 concentration and negative for CO_2. This suggests

that the oxygen reduction mechanism is qualitatively similar to that of state-of-the-art cathode listed in literature. Finally $LiNi_{0.8}Co_{0.2}O_2$ can be regarded as an alternative material to the conventional nickel oxide cathodes in molten carbonate fuel cells.

Also, Cobalt coated nickel electrodes were prepared by means of aqueous tape casting process using poly vinyl alcohol (PVA), glycerol and diperbyk^T as binder, plasticizer and dispersant respectively. Green tapes were sintered at 850^o C under reduced atmosphere. Impedance studies showed no mass transfer limitations in the initial stages of operation. Mass transfer process starts nearly after 20 hours after reaching the operating conditions. The magnitude of the impedance decreased as the operating time increased. Also, significant decrease in charge transfer resistance was also noticed with increase in time. Long-term stability tests revealed that the prepared material has a lower solubility in molten alkali carbonate melts when compared to the state-of-the-art nickel oxide cathodes. Hence, electrodes prepared using cobalt coated nickel powder can be used as an alternate to the conventional nickel oxide.

We have developed a three phase homogeneous model to simulate the performance of the molten carbonate fuel cell cathode. The homogeneous model is based on volume averaging of different variables in the three phases over a small volume element. This approach can be used to model porous electrodes as it represents the real system much better than the conventional agglomerate model. Using the homogeneous model the polarization characteristics of the MCFC cathode was studied under different conditions. Significant results obtained from the model are summarized below:

- The electrolyte conductivity and exchange current density have very large effect on the performance of MCFC cathode as compared to other parameters. Due to low electrolyte conductivity as compared to solid phase conductivity, most of the polarization loss occurs in a region close to the electrolyte matrix. Most of the material within the center of the electrode does not take part in the electrochemical reaction. This leads to low active material utilization within the electrode. Both low electrode and electrolytic conductivity lead to very poor reaction rate distribution across the electrode.
- Increase in reaction rate as exemplified by the exchange current density leads to decrease in polarization losses. Further, with increase in i_o the polarization loss increases linearly with increasing applied loads. However, at low values of i_o the

polarization loss increases asymptotically and reaches a plateau with increase in current.

- The amount of active material utilized also varies with exchange current density. At high values of i_0 (> 10 mA/cm^2), irrespective of the applied load most of the reaction takes place in a small part of the electrode near the separator and hence only 5% of the electrode is utilized. For small i_o values the reaction rate is slow and hence this allows sufficient time for dissolved O_2 and CO_2 to reach the active solid interface and react. The slow reaction rate also allows the reaction to take place much deeper within the electrode as compared to at high reaction rates. Both these factors contribute to the higher utilization observed for low i_o values.
- Changes in both gas phase and liquid phase diffusion coefficient do not have a significant effect on the polarization characteristics. In general, in the polarization curve an upward bending effect is observed due to kinetic limitations and a downward bending effect due to mass transfer limitations. Under normal operating conditions mass transfer is not rate limiting and the electrode is generally under mixed control.
- The diffusion coefficients, electrolyte conductivity and the exchange current density are all affected by changes in temperature. All of them have an Arrhenius form of dependency on temperature. The activation energy and the frequency factor for each of these parameters have been estimated by fitting the model to experimental data of $LiNiCoO_2$ at different temperatures. Using these fitted parameters the performance of NiO and $LiCoO_2$ cathodes has been studied. Exchange current density for different materials was obtained by fitting the model to the experimental polarization data. Hence, apart from qualitative analysis of the cathode behavior, the model can be used to extract critical thermodynamic, kinetic and transport parameters from polarization data.

A key parameter whose effect on the behavior of the electrode has not been considered is electrolyte filling. Increasing the amount of electrolyte within the MCFC cathode increases the conductivity but reduces the mass transfer rate. Simulations were run by increasing $\varepsilon^{(l)}$ and decreasing $\varepsilon^{(g)}$ to account for the increase in electrolyte fill. Results from our model show that the polarization drops with increasing electrolyte filling. There was no optimum as seen

experimentally. The model simulations were obtained by keeping all parameters except the porosities constant. Any modification to the electrolyte content will change the interfacial surface areas (a^{sl} and a^{gl}), which has not been accounted for in these simulations. Mercury porosimetry yields information on the active surface areas corresponding to micropores and macropores and also the liquid and gas porosity. Assuming that the micropores are flooded with electrolyte and macropores with gas, we can determine values for a^{sl} and a^{gl}. These two parameters along with the porosities can be input into the model to determine the polarization behavior. In future, we plan to extend the homogeneous model to account for electrolyte filling by using data from mercury porosimetry.

REFERENCES

[1]. P. Zegers, in: Proceedings of the Conference on the Role of Fuel Cells in a Sustainable Energy Supply, Madrid, July 2001.

[2] Fuel Cell Handbook, 5th Edition, EG&G Services Parsons, Inc., Science Applications International Corporation, National Energy Technology Laboratory, Morgatown, WA, 2000, pp. 9–70.

[3] A. Dicks, A. Siddle, *J. Power Sources* 86 (2000) 316–323.

[4] B. Bosio, P. Costamagna, F. Parodi, B. Passalacqua, *J. Power Sources* 74 (1998) 175–187.

[5] E. Arato, B. Bosio, R. Massa, F. Parodi, *J. Power Sources* 86 (2000), 302–308.

[6] M. Pokojski, B. Aktiengesellschaft, in: Proceedings of the 6th Grove Fuel Cell Symposium, London, September 1999.

[7] P.H. Eichenberger, *J. Power Sources* 71 (1998) 95–99.

[8] R.A. Figueroa, J. Otahal, *J. Power Sources* 71 (1998) 100–104.

[9] T. Ishikawa, H. Yasue, in: Proceedings of the 6th Grove Fuel Cell Symposium, London, September 1999.

[10] Th. Brenscheidt, F. Nitschke´, O. So¨llner, H. Wendt, *Electrochim. Acta* 46 (2001) 783–797.

[11] L. Plomp, E.F. Sitters, C. Vessies, F.C. Eckes, *J. Electrochem. Soc*. 138 (1991) 629–630.

[12] G. Kucera, K. Myles, A. Brown, M. Roche, D. Chu, E. Indacochea, in: Proceedings of the Fourth Annual Fuel Cells Contractors Review Meeting, US DOE/METC, 1992, pp. 31–41.

[13] L. Giorgi, E. Simonetti, M. Carewska, S. Scaccia, F. Zarzana, in: Proceedings of the Fuel Cell Seminar, 1994, pp. 172–175.

[14] J.B.J. Veldhuis, F.C. Eckes, L. Plomp, *J. Electrochem. Soc*. 139, (1992) 6–8.

[15] A. Lundblad, S. Schwartz, B. Bergman, *J. Power Sources* 90 (2000), 224–230.

[16] C. Lagergren, A. Lundblad, B. Bergman, *J. Electrochem. Soc*. 141, (1994) 2959–2966.

[17] L. Plomp, J.B.J. Veldhuis, E.F. Sitters, S.B. van der Molen, *J. Power Sources* 39 (1992) 369–373.

[18] S.T. Kuk, Y.S. Song, K. Kim, *J. Power Sources* 83 (1999) 50–56.

[19] B. Fang, H. Chen, *J. Electroanal. Chem*. 501 (2001) 128–131.

[20] T. Fukui, S. Ohara, H. Okawa, T. Hotta, M. Naito, *J. Power Sources*, **86** (2000) 340.

[21] X. Zhang, H. Okawa, T. Fukui, *Denki Kagaku*, **66**(11) (1998) 1141.

[22] S. T. Kuk, Y. S. Song, S. Suh, J. Y. Kim and K. Kim, *J. Mater. Chem*, 2001, 11, 630-635.

[23] S.W. Nam, S.G. Kim, I.H. Oh, T.H. Lim, H.Y. Ha, S.A. Hong, K. Kim and H.C. Lim, Carbonate Fuel Cell Technology, *Proceedings of the fifth International Symposium*, pv 99-20, 253-262.

[24] X. Zhang, P. Capobianco, A. Torazza, and B. Passalacqua, *Electrochemistry*, **67**(6) (1999).

[25] J. B. J. Veldhuis, F. C. Eckes, and L. Plomp, *J. Electrochem. Soc*., **139** (1) (1992) L6.

[26] K. Ota, Y. Takeishi, S. Shibata, H. Yoshitake, and N. Kamiya, *J. Electrochem. Soc*., **142**(10) (1995) 3322.

[27] Mohamedi, M.; Hisamitsu, Y.; Kihara, K.; Kudo, T.; Itoh, T.; Uchida, Isamu. *J. Alloys* Compd. (2001), 315 (1-2), 224-233..

[28] Lada, W.; Deptula, A.; Sartowska, B.; Olczak, T.; Chmielewski, A. G.; Carewska, M.; Scaccia, S.; Simonetti, E.; Giorgi, L.; Moreno, A., Mater. Res. Soc. Symp. Proc. (2000), 623 (Materials Science of Novel Oxide-Based Electronics) 395-400.

[29] G. Wilemski, *J. Electrochem. Soc.*, **130**, 117 (1983)

[30] C. Y. Yuh and J. R. Selman, *J. Electrochem. Soc.*, **131**, 2062 (1984)

[31] J. A. Prins-Jansen, J. D. Fehribach, K. Hemmes and J. H. W. de Wit, *J. Electrochem. Soc.*, **143**, 1617 (1996).

[32] P. de Vidts and R. E. White, *J. Electrochem. Soc.*, **144**, 1343 (1997).

[33] R. D. Shannon, G. T. Prewitt, *Acta Crystallogr*., Sect. B 25 (1969) 925.

[34] F. J. Perez, D. Duday, M. P. Hierro, C. Gomez, M. Romero, M. T. Casais, J. A. Alonso, M. J. Martinez and L. Daza, *Journal of Power Sources,* 86 (2000), 309.

[35] Salam, Loey A.; Matthews, Richard D.; Robertson, Hugh, Journal of the European Ceramic Society (2000), 20(9), 1375-1383.

[36] C. Y. Yuh and J. R. Selman, *J. Electrochem. Soc*., **138**(12), (1991) 3642.

[37] C. Y. Yuh and J. R. Selman, *J. Electrochem. Soc*., **138**(12), (1991) 3649.

[38] A. Durairajan, H. Colon, B. Haran, R. E. White and B. N. Popov, *J. Power Sources,* **104** (2), (2002), 157-168.

[39] G. L. Lee, J. R. Selman and L. Pomp, *J. Electrochem. Soc.*, **140**, 390 (1993).

[40] J. S. Newman and C. W. Tobias, *J. Electrochem. Soc.*, **109**, 1183 (1962).

[41] E. Fontes, M. Fontes and D. Simonsson, *Electrochem. Acta*, **141**, 1 (1996).

[42] E. L. Cussler, Diffusion, Mass Transfer in Fluid Systems, New York, (1984).

[43] C. Lagergren and D. Simonsson, *J. Electrochem. Soc.*, **144**, 3813 (1997).

[44] H. R. Kunz and L. A. Murphy, *J. Electrochem. Soc.*, **135**, 1124 (1988).

Table I. List of parameters used in model simulations.

Parameter	Value	Reference
Diffusion coefficient of CO_2 in the liquid phase, $D_{CO_2}^{(l)}$	$1e^{-3}$ cm^2/s	[31]
Diffusion coefficient of CO_2 in the liquid phase, $D_{O_2}^{(l)}$	$3e^{-3}$ cm^2/s	[31]
Diffusion coefficient of CO_2 in the gas phase, $D_{CO_2}^{(g)}$	1.16 cm^2/s	[42]
Diffusion coefficient of O_2 in the gas phase, $D_{O_2}^{(g)}$	1.16 cm^2/s	[42]
Electrode conductivity, σ	13 S/cm	[39]
Electrode conductivity, κ	$2.0e^{-2}$ S/cm	[31]
Correction for diffusion coefficient, b	1.5	[32]
Correction for conductivity, d	1.5	[32]
Specific surface area at the liquid/solid interface, $a^{(sl)}$	$2e^4$ cm^2/cm^3	
Specific surface area at the liquid/gas interface, $a^{(lg)}$	4000 cm^2/cm^3	
Equilibrium constant relating the concentration of CO_2 in the liquid and gas phase, K_{e,CO_2}	0.01	
Equilibrium constant relating the concentration of O_2 in the liquid and gas phase, K_{e,O_2}	0.01	
Rate constant of the molar flux of CO_2 between the liquid and gas phase, $k_{CO_2}^{(lg)}$	$3e^{-3}$ cm/s	
Rate constant of the molar flux of O_2 between the liquid and gas phase, $k_{O_2}^{(lg)}$	$2e^{-3}$ cm/s	
Thickness of the electrode, L	0.06 cm	Measured
Liquid porosity, $\varepsilon^{(l)}$	0.3	Measured
Gas porosity, $\varepsilon^{(g)}$	0.4	Measured
Solid porosity, $\varepsilon^{(s)}$	0.3	Measured
Exchange current density, i_0^0	50 mA/cm^2	[39]

Cathodic transfer coefficient, α_c	0.5	[31,36]
Cathodic transfer coefficient, α_a	1.5	[31,36]
r_1	-1.25	[31]
r_2	0.375	[31]

Table II. Temperature dependence of different electrode parameters for $LiNiCoO_2$ cathode.

	a	**b (1/K)**	**R^2**
κ	3.268 S/cm	4715.5	0.9915
$D^l_{CO_2}$	144.82 cm^2/s	10975	0.9994
$D^l_{O_2}$	0.352 cm^2/s	4417	0.9751
i_0	243.96 A/cm^2	11887	0.9842

Table III. Kinetic and conductivity properties for different cathode materials.

	σ (S/cm)	**i_o (mA/cm^2)**
NiO	13	50
$LiCoO_2$	1	5
$LiNiCoO_2$	5	0.65

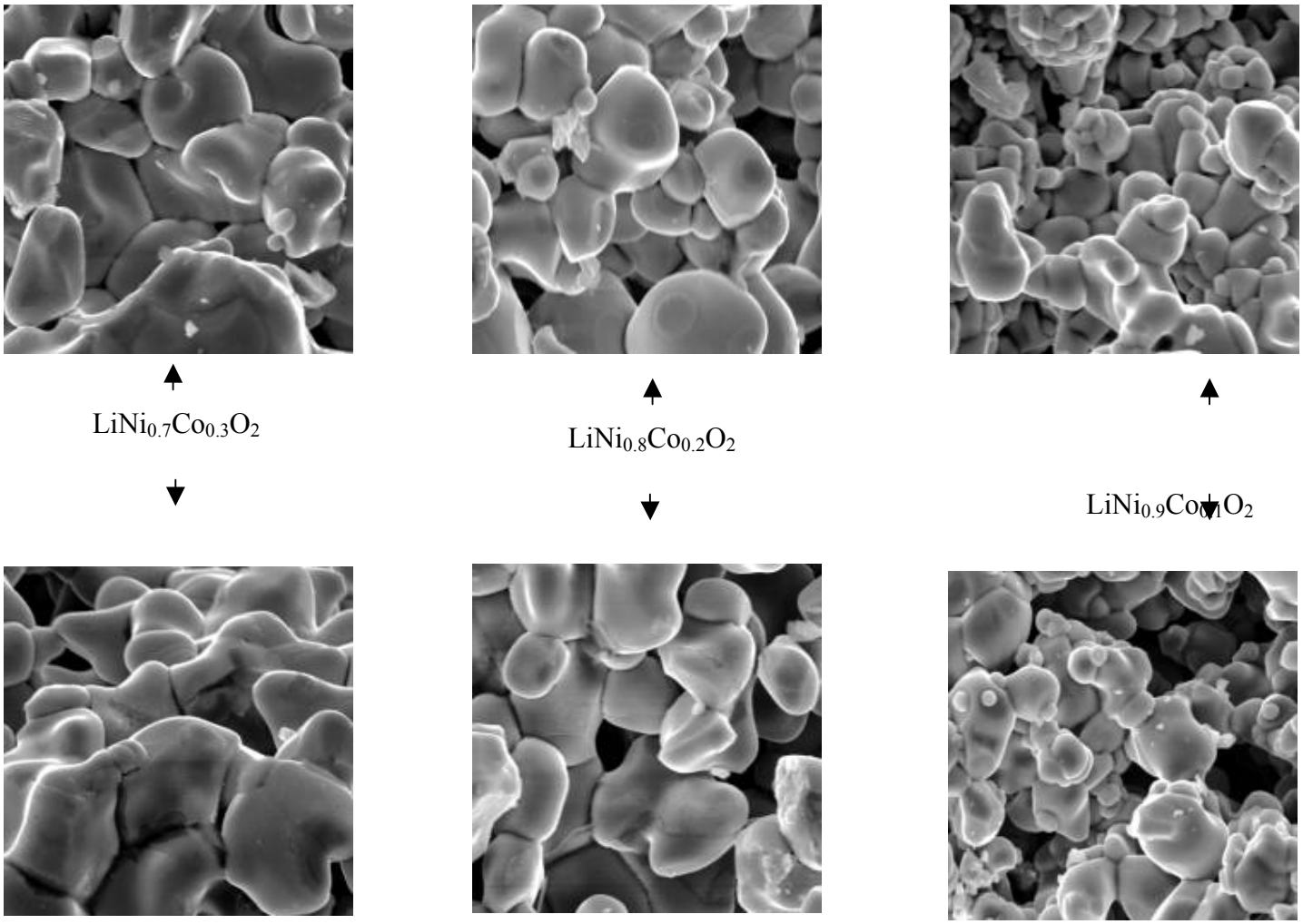

Figure 1 SEM images of synthesized $LiLi_{0.8}Co_{0.2}O_2$ solid solutions

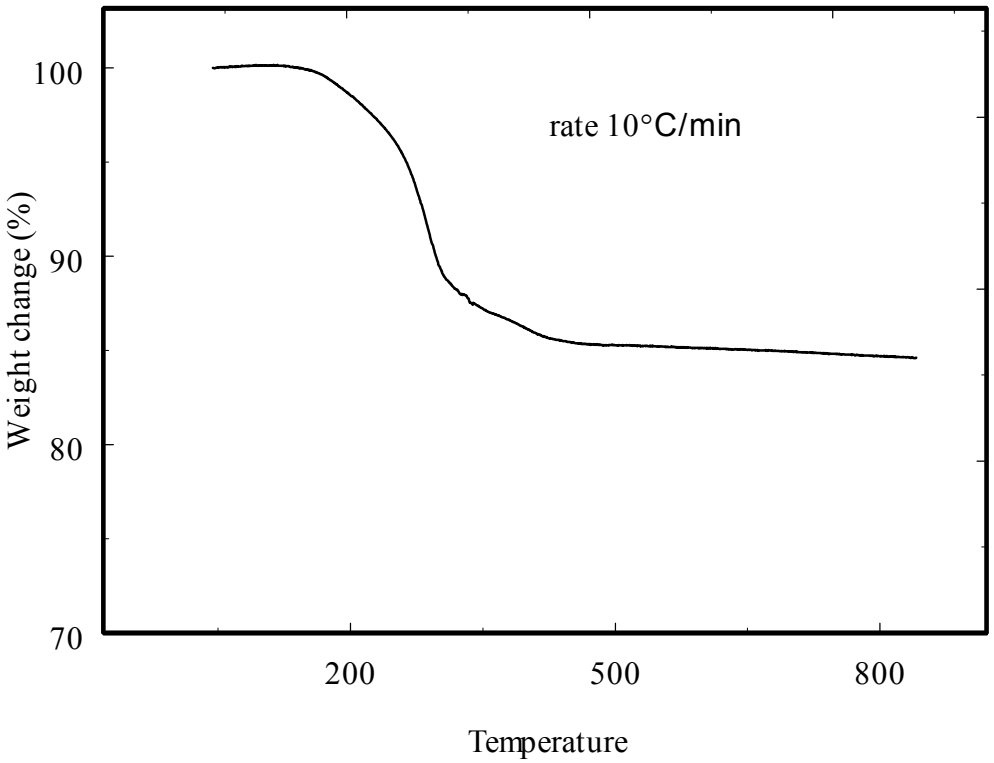

Figure 2. TGA of $LiLi_{0.8}Co_{0.2}O_2$ green tape

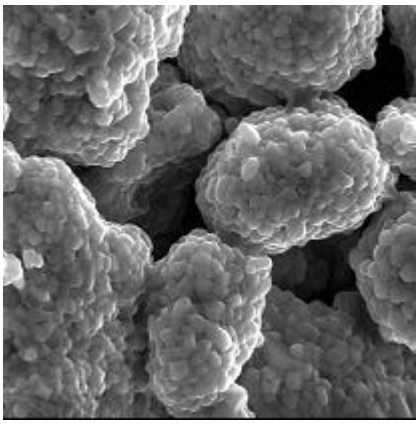

800° C 5.7 μm

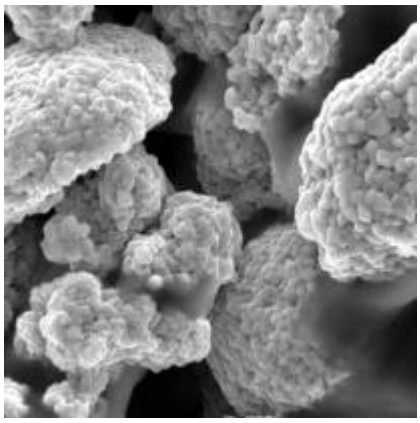

850° C 5.7 μm

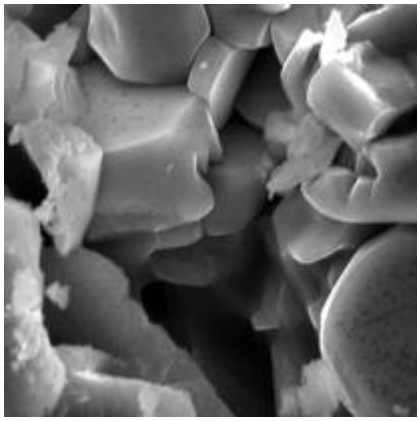

900° C 5.7 μm

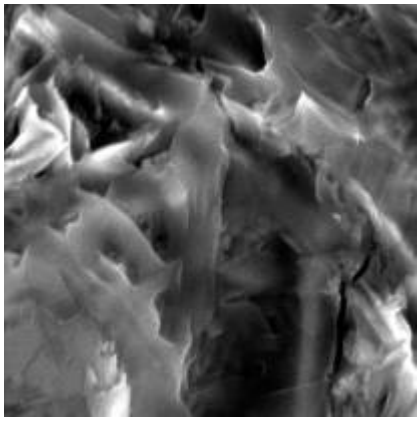

1000° C 5.7 μm

Figure 3 SEM images of $LiLi_{0.8}Co_{0.2}O_2$ electrode sintered in air at different temperatures

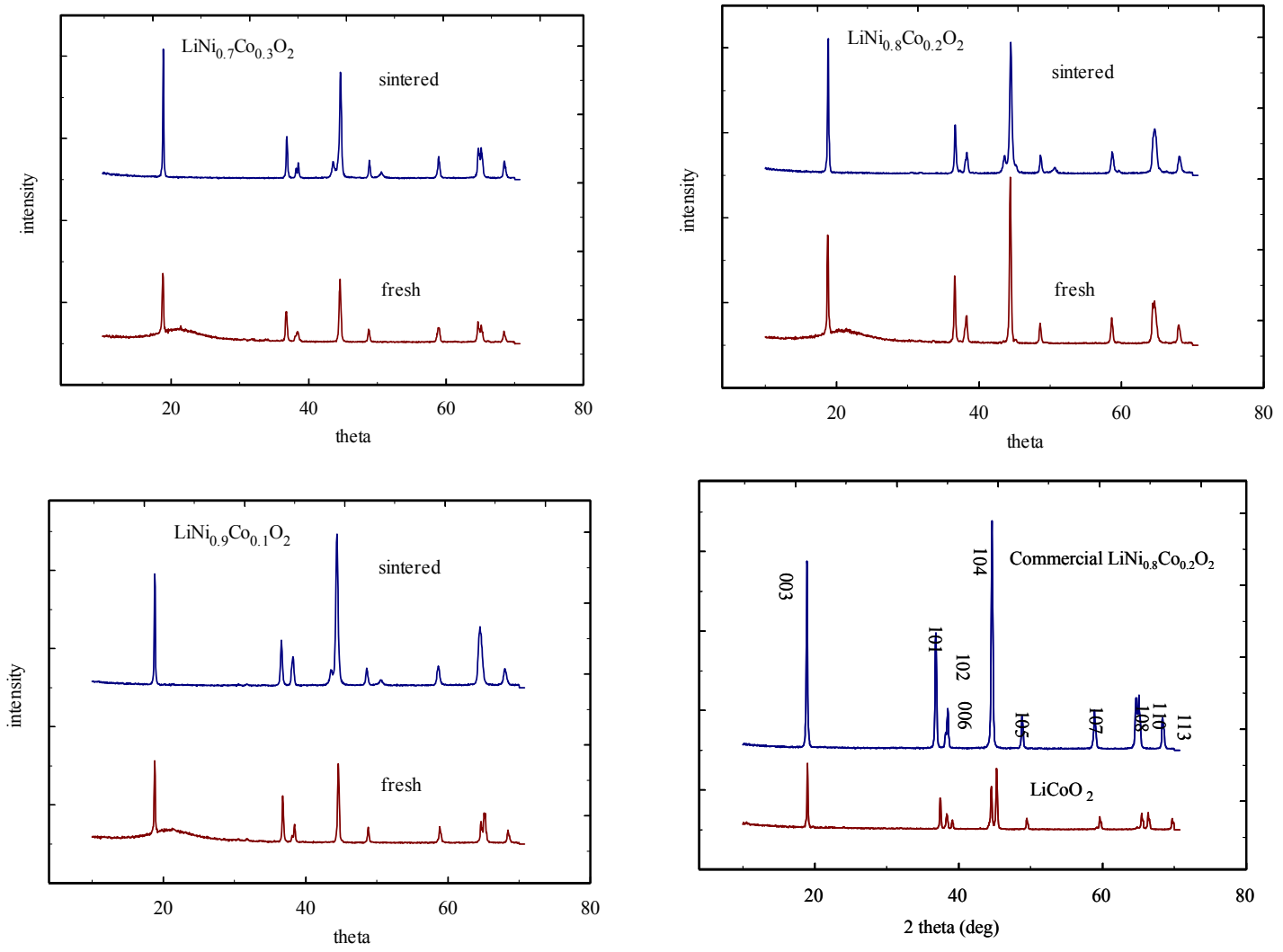

Figure 4 X-ray diffraction patterns of pristine $LiCoO_2$ and $LiNi_xCo_{1-x}O_2$ solid solutions obtained by solid-state reaction procedure from lithium nitrate, nickel hydroxide and cobalt oxalate precursors. The XRD pattern of commercial $LiNi_{0.8}Co_{0.2}O_2$ is shown for comparison.

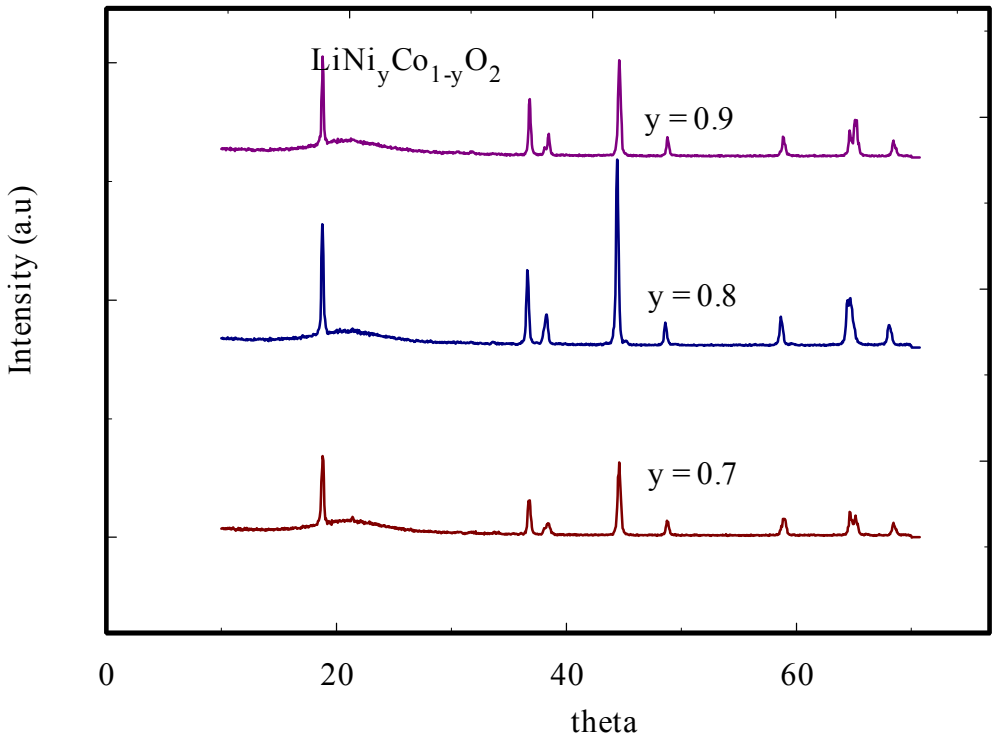

Figure 5. X-ray diffraction patterns of $LiNi_xCo_{1-x}O_2$ mixed oxides after sintering in air at 800°C for 24 hours

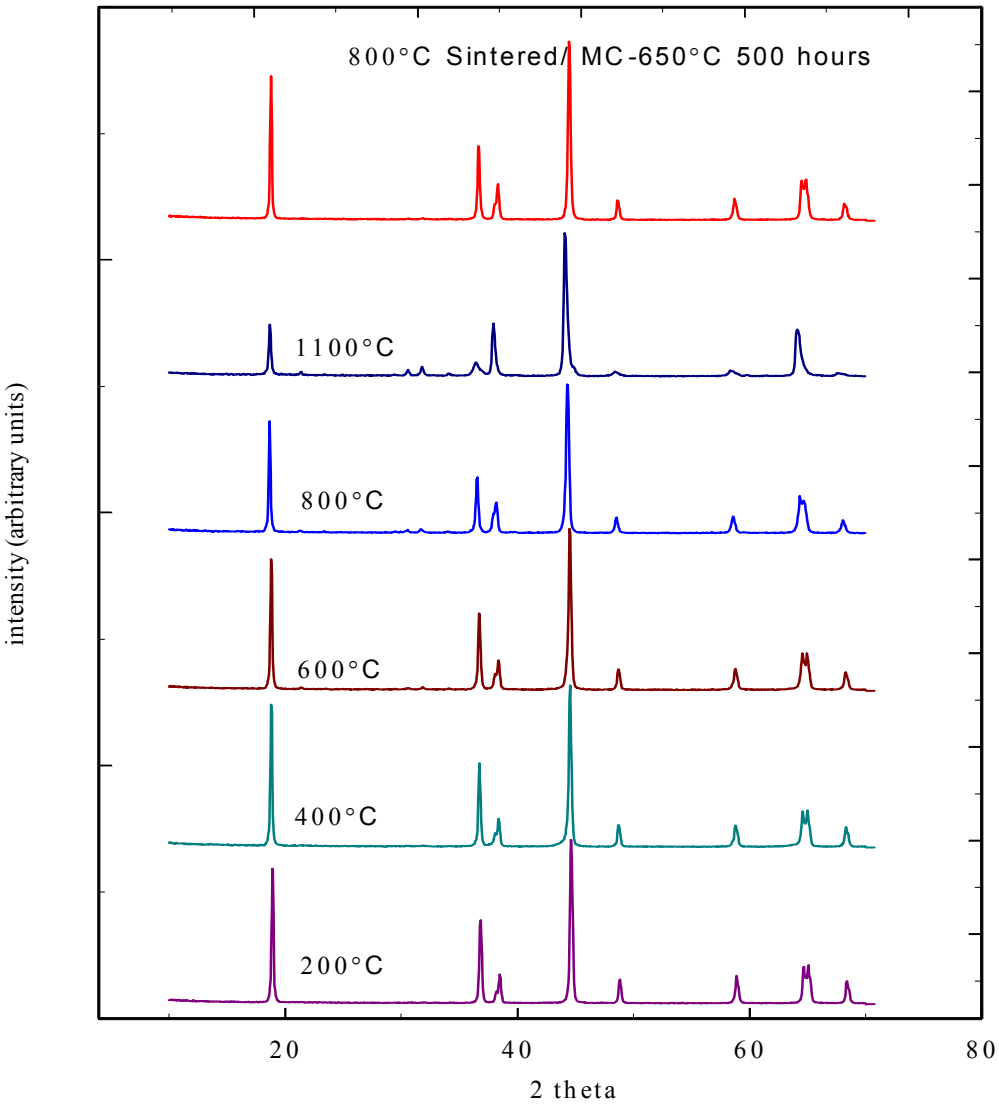

Figure. 6. X-ray diffraction patterns of $LiNi_{0.8}Co_{0.2}O_2$ mixed oxides after sintering at different temperatures in air 24 hours. $LiNi_{0.8}Co_{0.2}O_2$ sintered in molten carbonate eutectic at 650°C for 500 hours is shown for comparison.

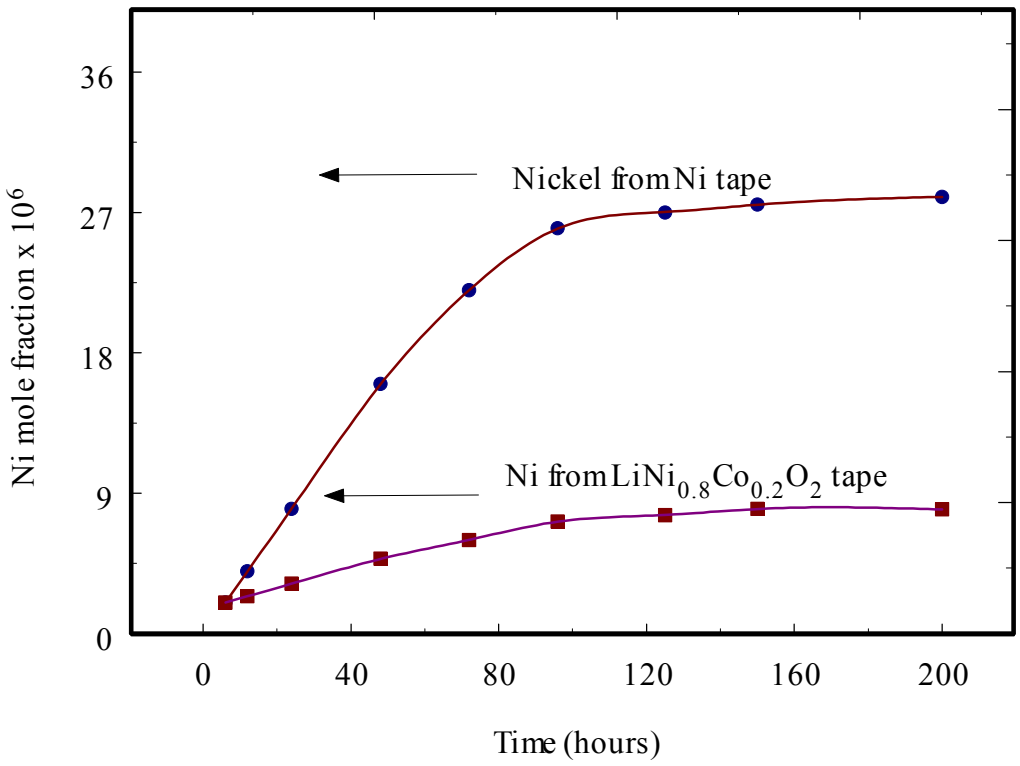

Figure 7. Atomic absorption spectroscopy analysis of dissolved nickel in molten carbonate melt coming from $LiNi_{0.8}Co_{0.2}O_2$ electrodes during immersion tests

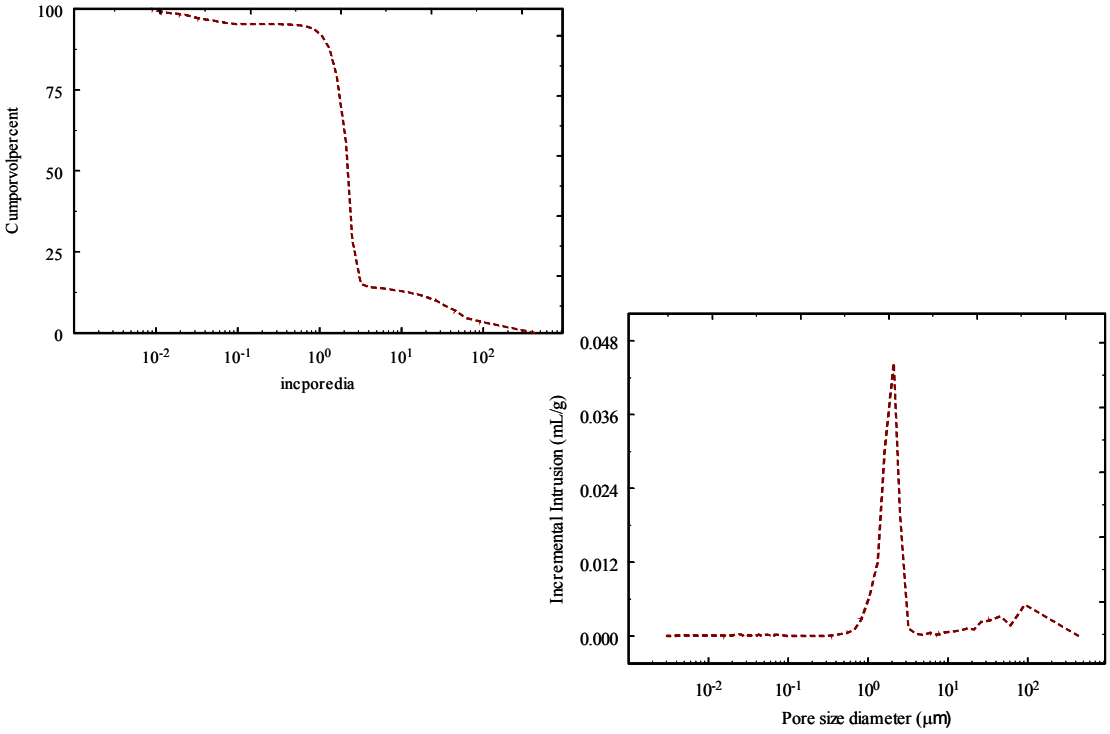

Figure 8. Pore volume distribution obtained on $LiNi_{0.8}Co_{0.2}O_2$ electrodes by mercury intrusion method.

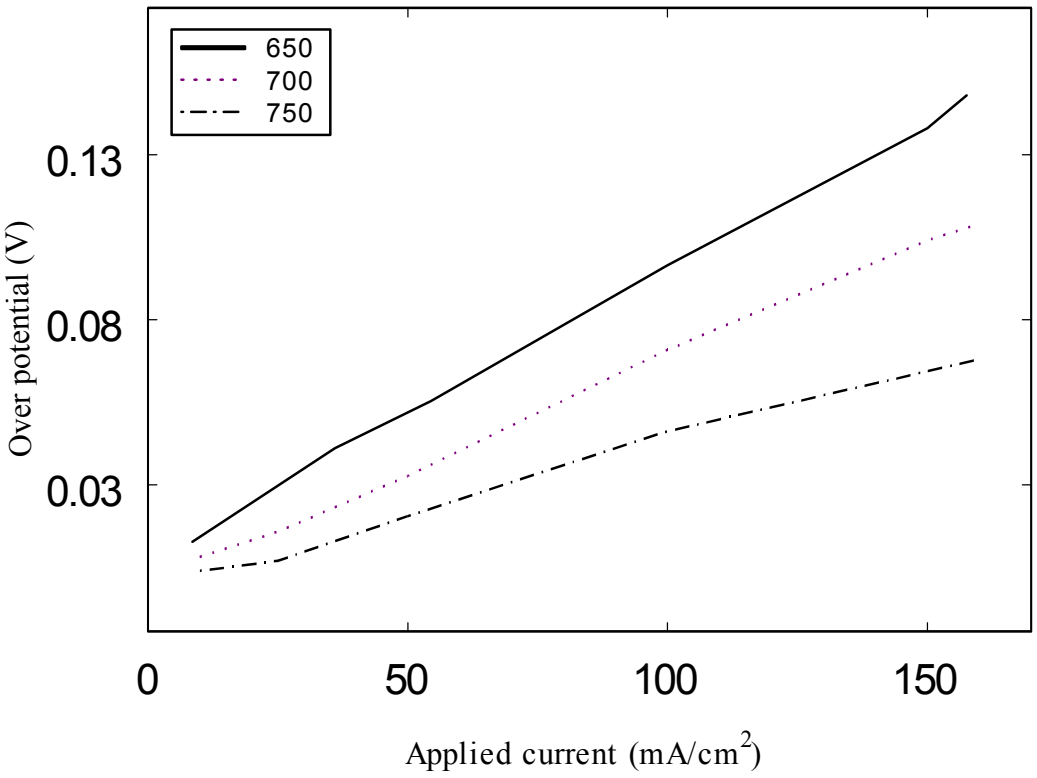

Figure 9. Comparison of Cathode polarization behaviors at different current loads for $LiNi_{0.8}Co_{0.2}O_2$ cathodes at different temperatures.

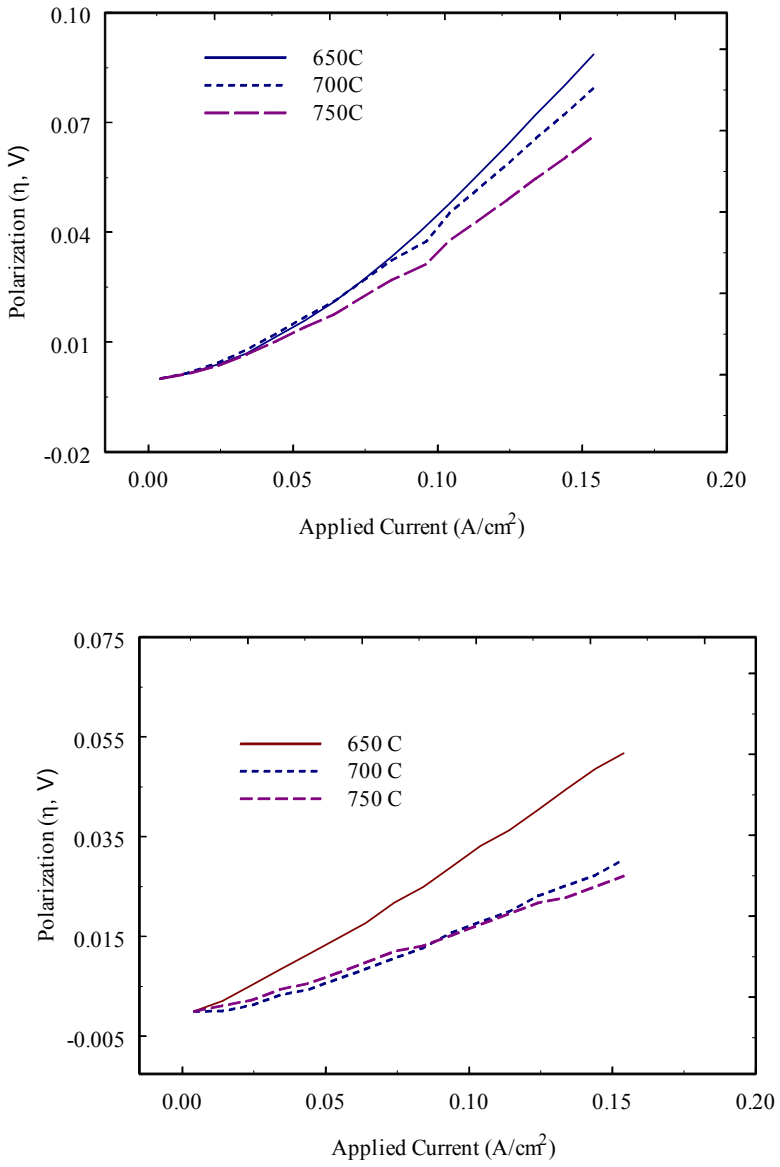

Figure 10. Polarization behavior of Nickel (a, top) and cobalt encapsulated nickel (b, bottom) electrodes at different operating temperatures

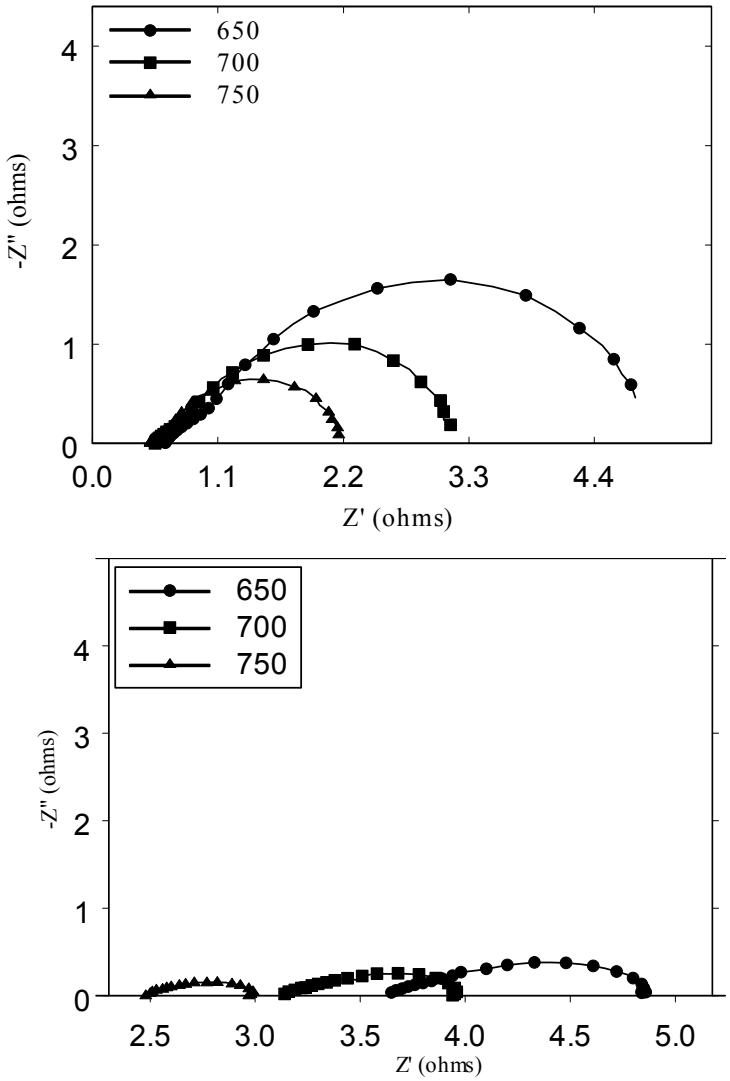

Figure 11. Nyquist plots of $LiCoO_2$ (a, top) and NiO (b, bottom) at different operating temperatures in standard cathode gas atmosphere.

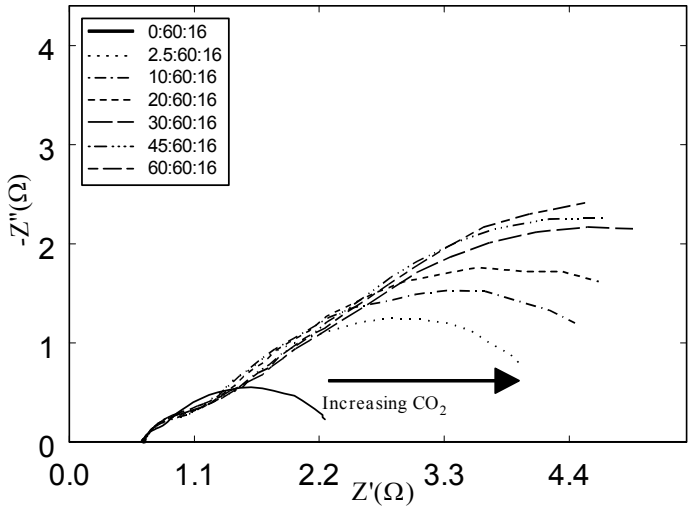

Fig. 12(a) 650° C

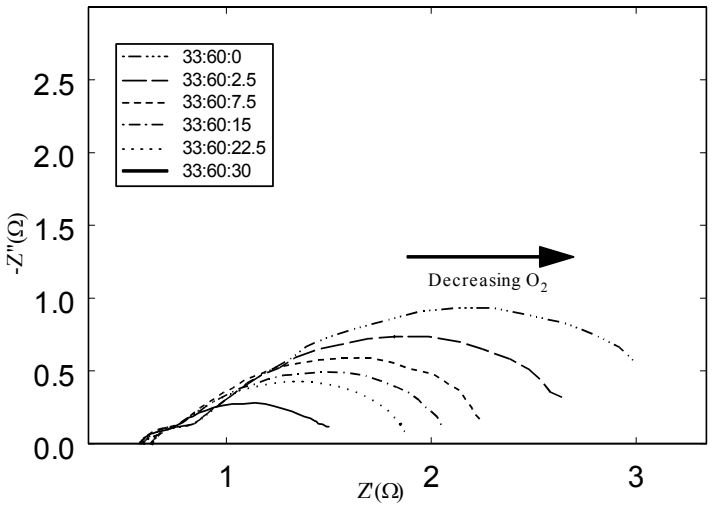

Fig. 12(b)

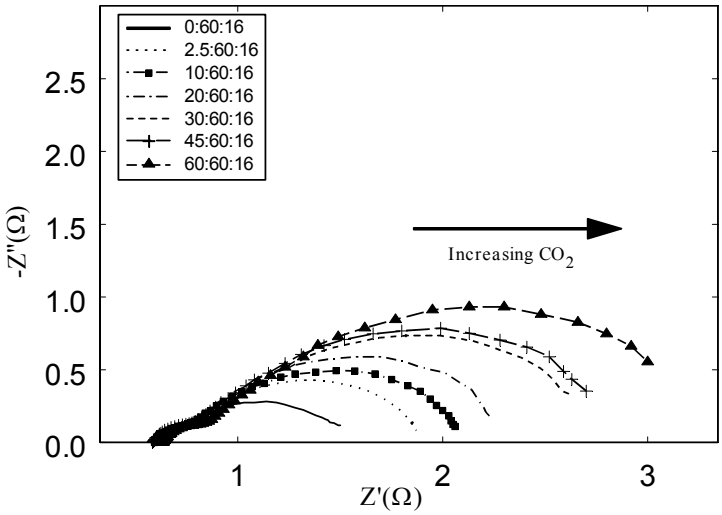

Fig. 12(c) 700° C

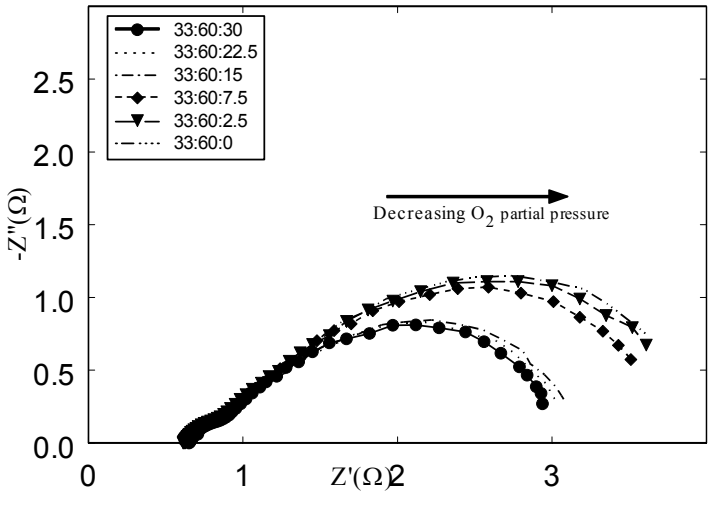

Fig. 12(d)

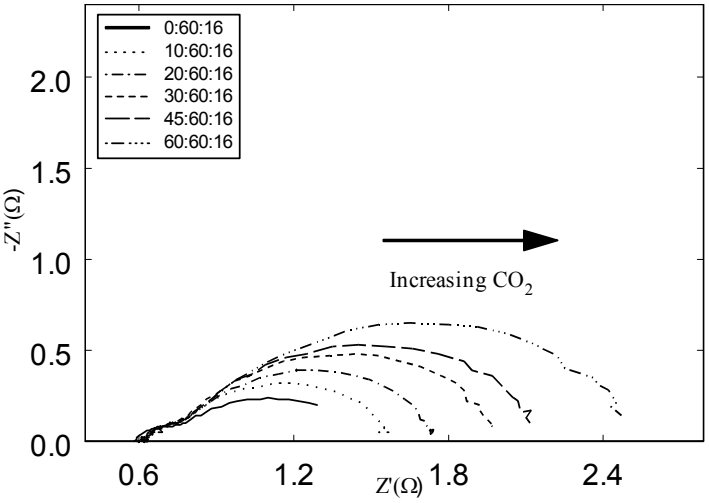

Fig. 12(e) 750° C

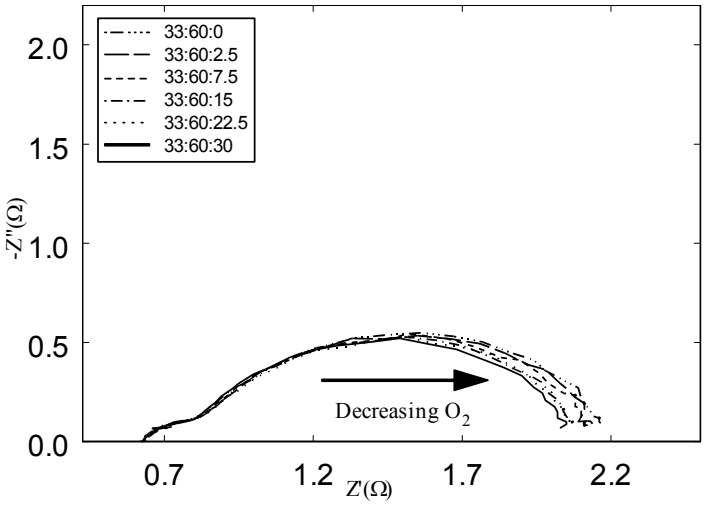

Fig. 12(f)

Figure 12. Nyquist plots of impedance response of $LiNi_{0.8}Co_{0.2}O_2$ electrode as a function of O_2 and CO_2 partial pressures at 650°C (a & b) and 700°C (c & d) 750° C (e & f) (the numbers in parenthesis "{}" indicates the CO_2, N_2 and O_2 concentrations in cc/min).

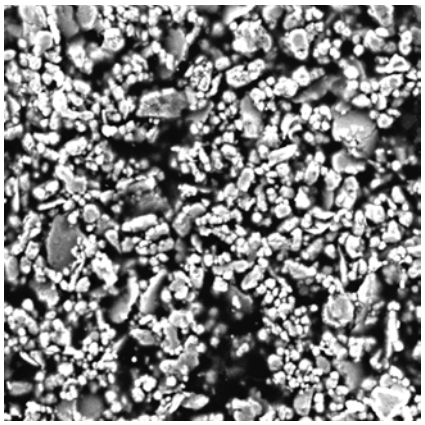

X1000

SEM of Tape cast Co coated nickel green tape

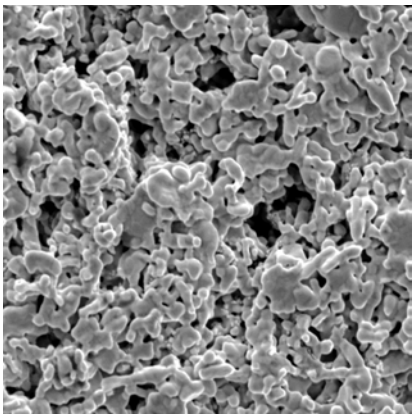

X1000

SEM of Tape cast Co coated sintered nickel electrode

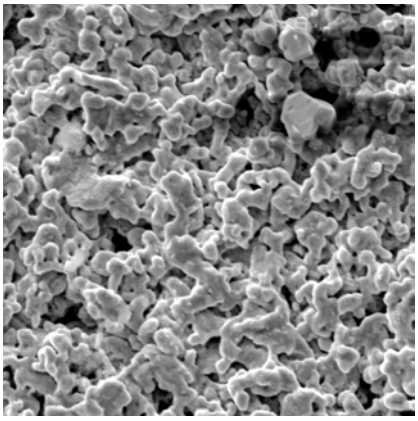

X 1000

SEM of tape cast Co coated Ni electrode after immersion in molten carbonate for 24 h.

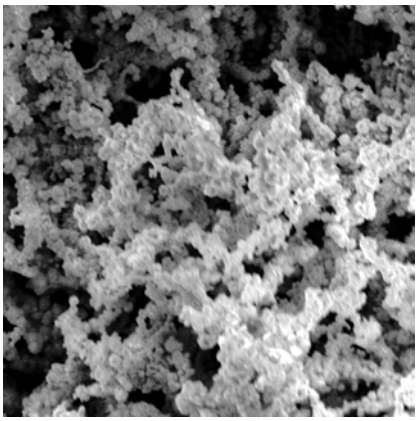

X 1000

SEM of Co coated Ni powder

Figure 13. SEM images of tape cast cobalt coated Ni electrodes.

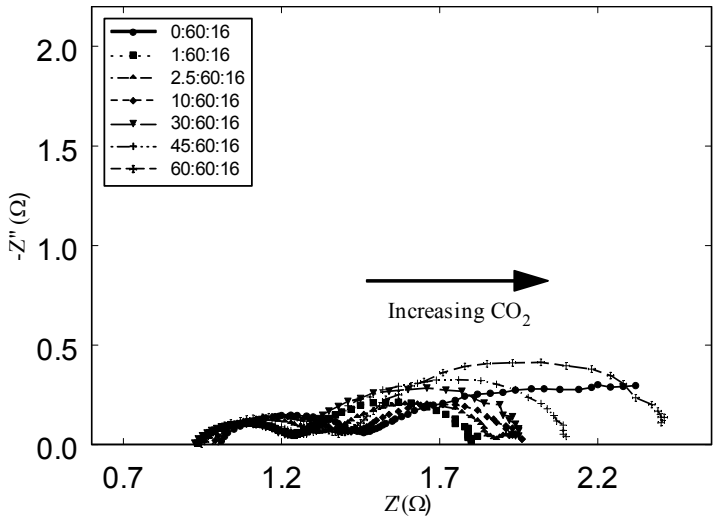
0:60:16
1:60:16
2.5:60:16
10:60:16
30:60:16
45:60:16
60:60:16
Increasing CO_2
-Z'' (Ω)
Z'(Ω)
0.0
0.5
1.0
1.5
2.0
0.7
1.2
1.7
2.2

(a)

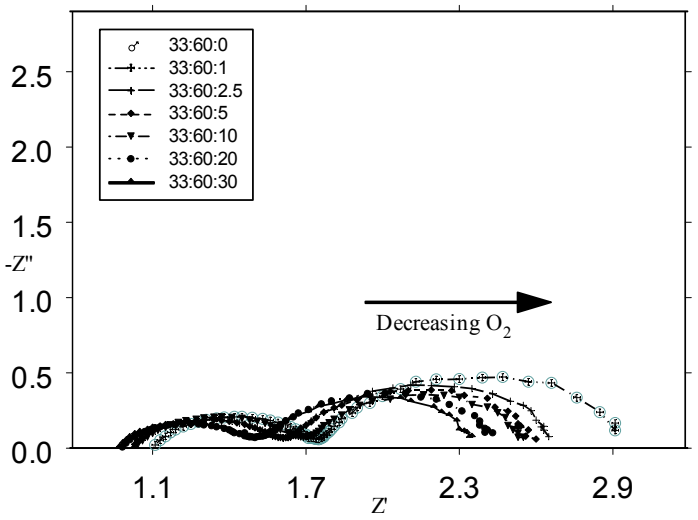
33:60:0
33:60:1
33:60:2.5
33:60:5
33:60:10
33:60:20
33:60:30
Decreasing O_2
-Z''
Z'
0.0
0.5
1.0
1.5
2.0
2.5
1.1
1.7
2.3
2.9

(b)

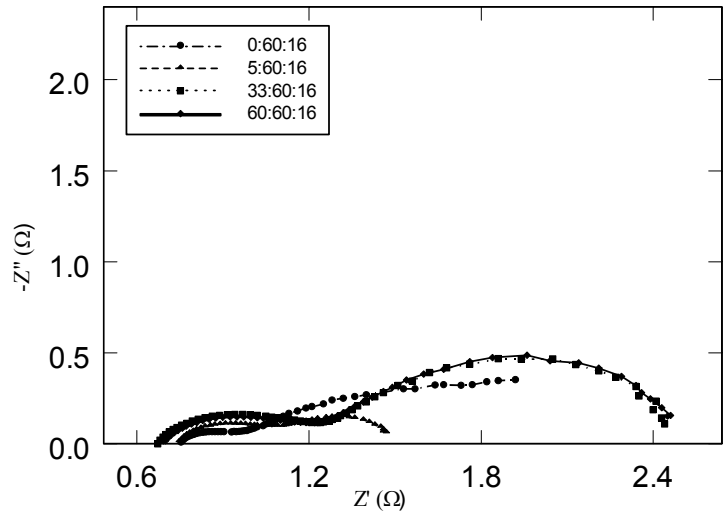
0:60:16
5:60:16
33:60:16
60:60:16
-Z'' (Ω)
Z' (Ω)
0.0
0.5
1.0
1.5
2.0
0.6
1.2
1.8
2.4

(c)

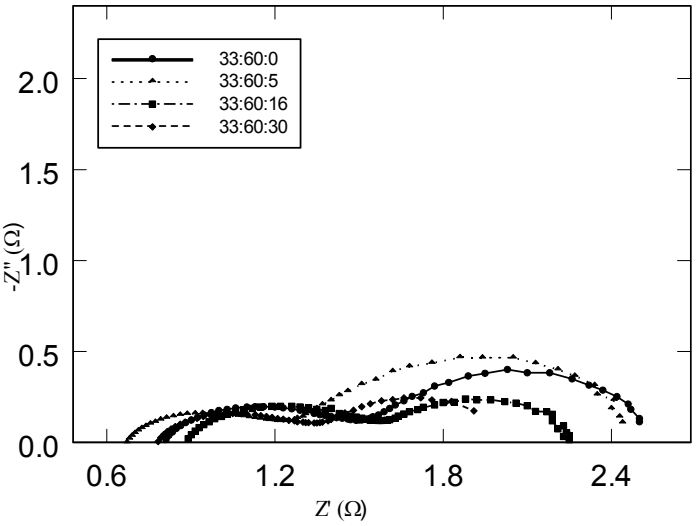
33:60:0
33:60:5
33:60:16
33:60:30
-Z'' (Ω)
Z' (Ω)
0.0
0.5
1.0
1.5
2.0
0.6
1.2
1.8
2.4

(d)

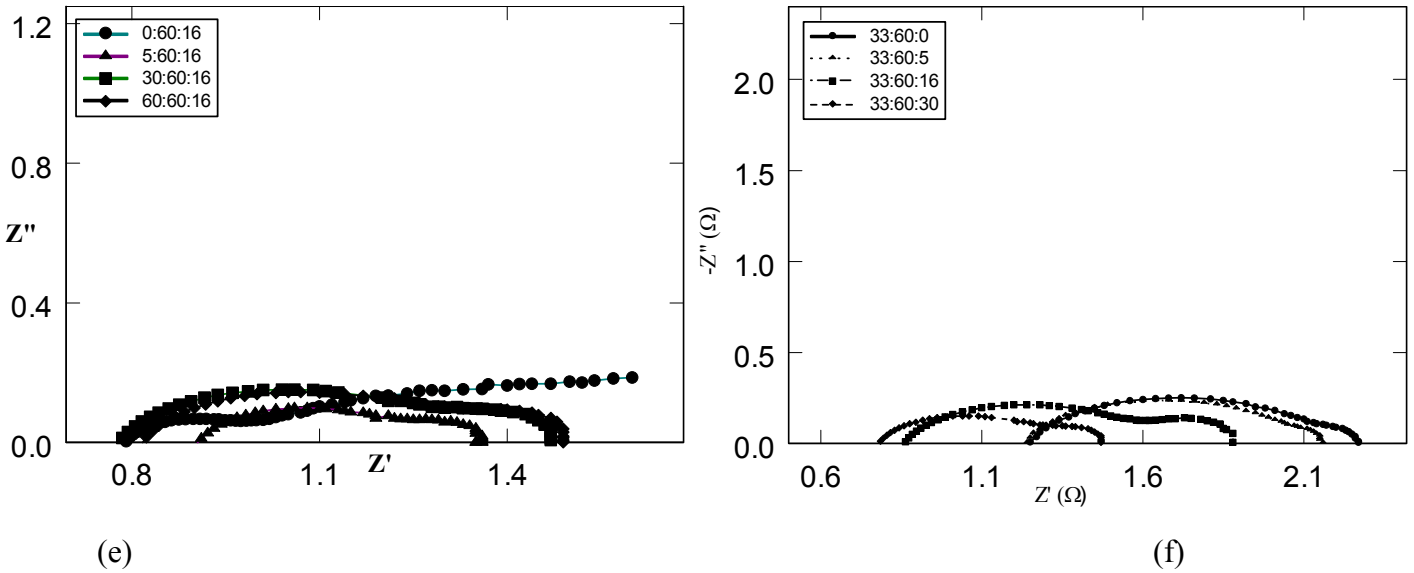

(e) (f)

Figure. 14. Impedance behavior of tape cast Co coated nickel electrode at 650^{o} (a & b), 700^{o} (b & c) and 750^{o} C (e & f)

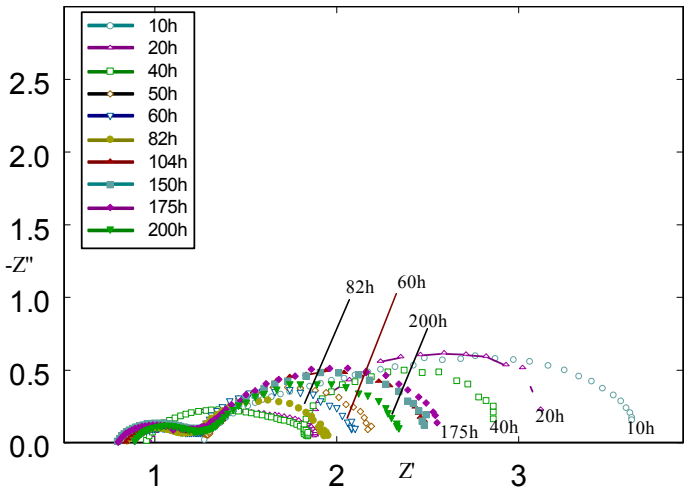

Figure 15. Impedance behavior of tape cast Co coated nickel electrode after different time of operation

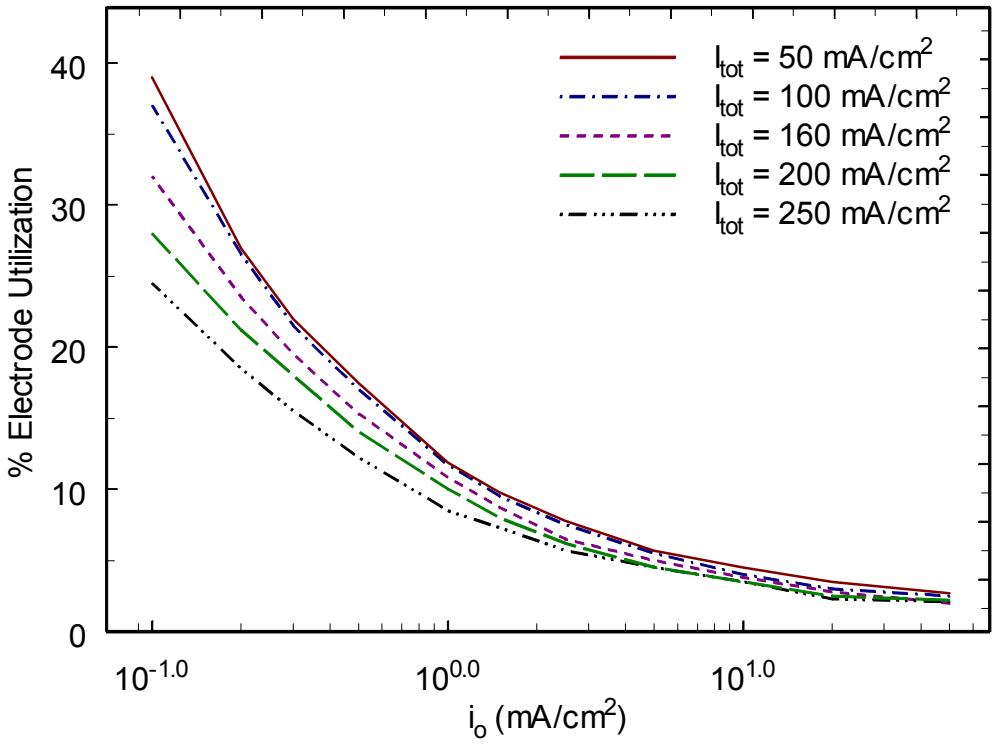

Figure 16. Change in the electrode utilization as a function of exchange current density. Profiles are shown for different applied currents

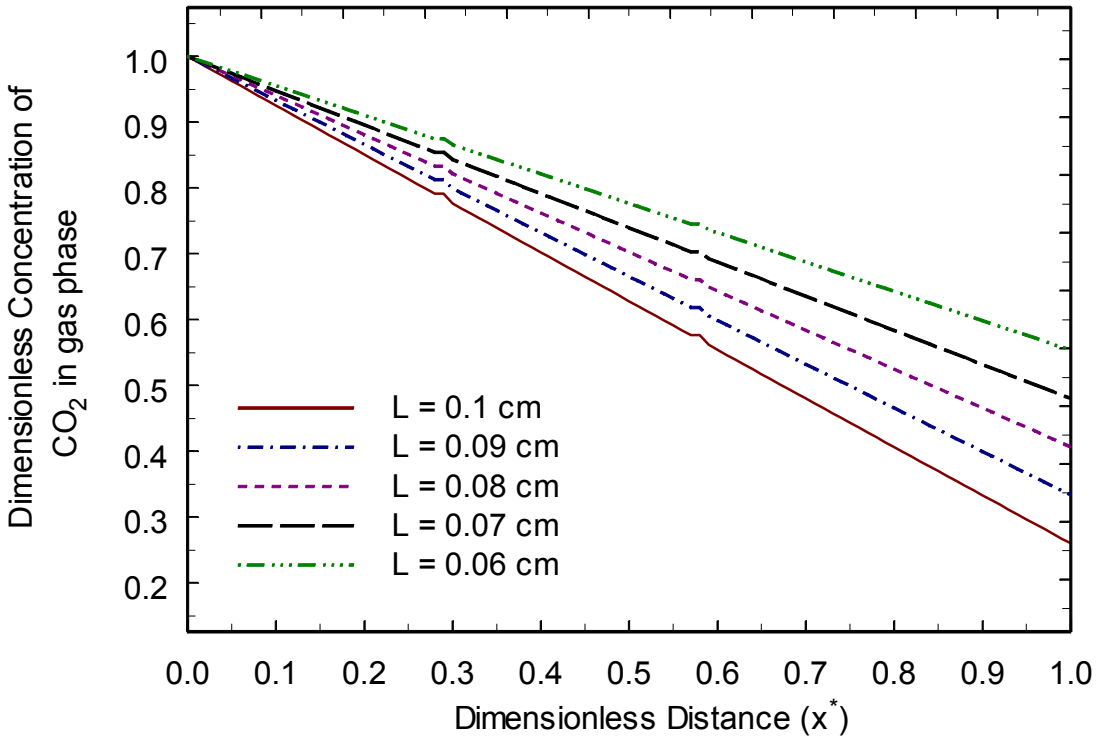

Figure 17. Change in the gas phase CO_2 concentration for varying electrode thickness

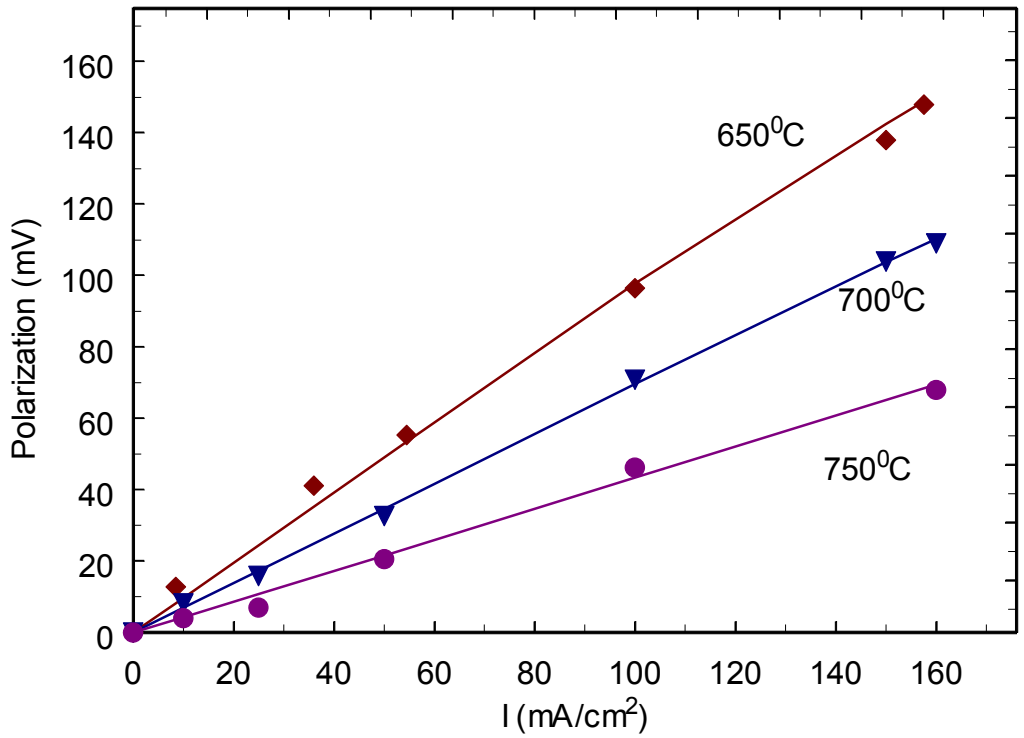

Figure 18. Change in $LiNiCoO_2$ electrode polarization with applied current density for different temperatures. Solid lines are model simulations and dots are experimental data. Thermodynamic, kinetic and transport parameters extracted from the fitting are presented in Table II

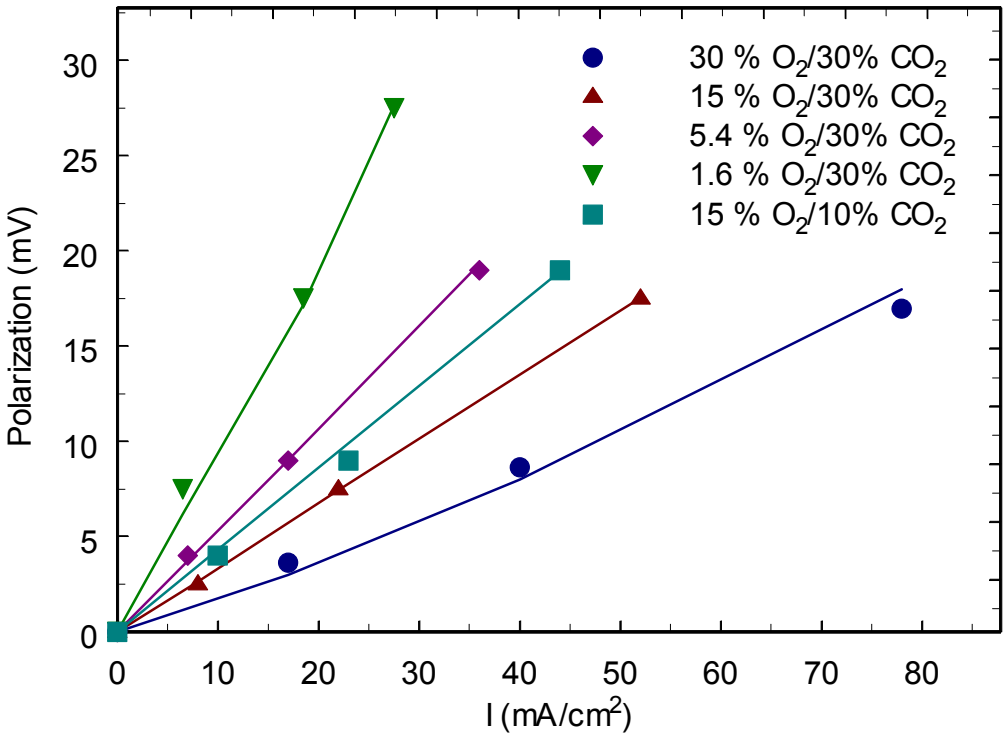

Figure 19. Comparison of model results and experimental data for different gas compositions. Experimental data were obtained from the polarization behavior for $LiCoO_2$ given by Lagergren and Simonsson (19)

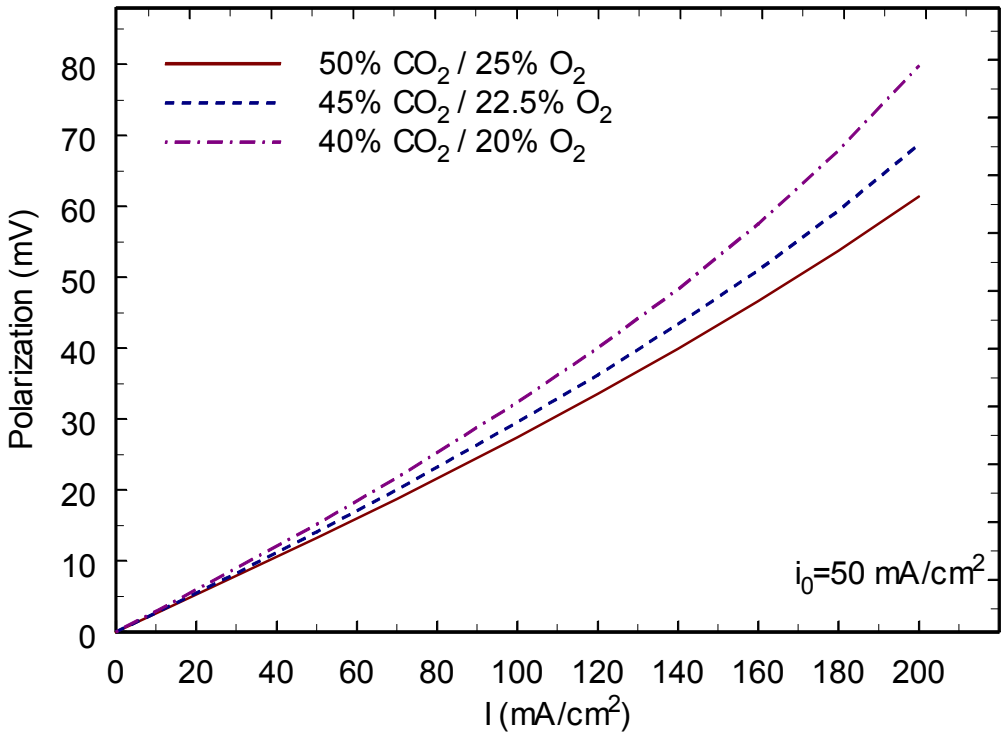

Figure 20. Effect of inert gas (N_2) on the polarization behavior of MCFC cathode

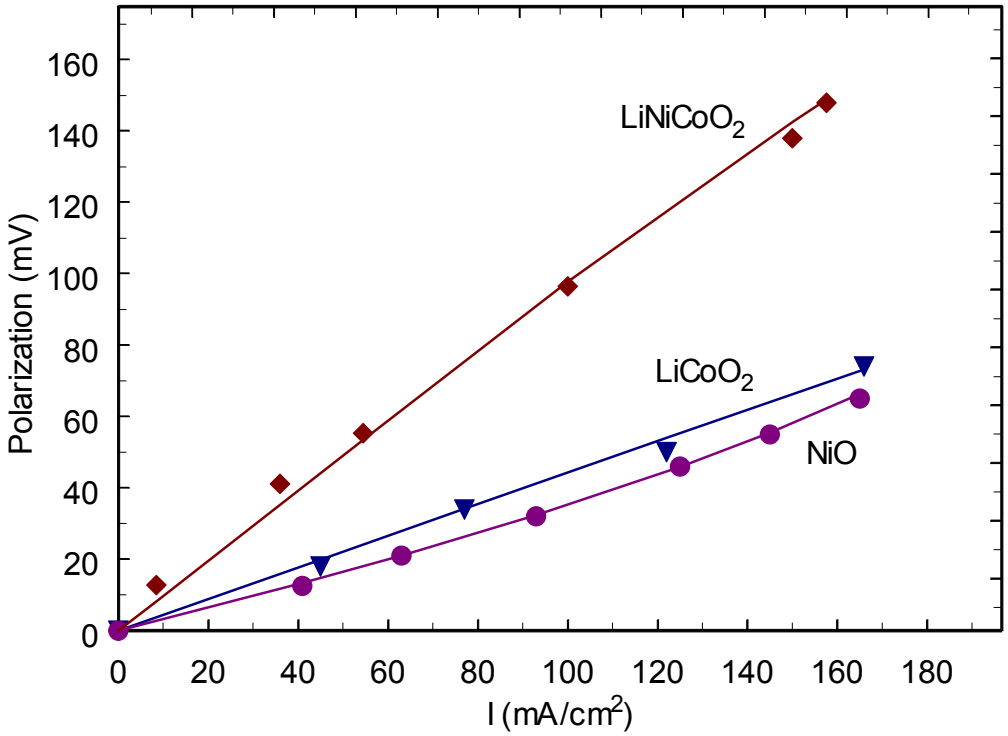

Figure 21. Comparison of model to experimental polarization data for different cathode materials